

**MASARYKOVA UNIVERZITA**  
**PŘÍRODOVĚDECKÁ FAKULTA**  
ÚSTAV TEORETICKÉ FYZIKY A ASTROFYZIKY

# **Bakalářská práce**

**BRNO 2022**

**VERONIKA BARTOŠOVÁ**



# **Studium změn orientace a pasivní stabilizace CubeSatů**

Bakalářská práce

**Veronika Bartošová**

**Vedoucí práce: Mgr. Filip Münz, PhD. Brno 2022**



# Bibliografický záznam

<b>Autor:</b>	Veronika Bartošová Přírodovědecká fakulta, Masarykova univerzita Ústav teoretické fyziky a astrofyziky
<b>Název práce:</b>	Studium změn orientace a pasivní stabilizace CubeSatů
<b>Studijní program:</b>	Fyzika
<b>Studijní obor:</b>	Astrofyzika
<b>Vedoucí práce:</b>	Mgr. Filip Münz, PhD.
<b>Akademický rok:</b>	2019/2022
<b>Počet stran:</b>	xv + 50
<b>Klíčová slova:</b>	určení orientace, GRBA $\alpha$ , nanosatelit, pasivní stabilizace, senzory



# Bibliographic Entry

<b>Author:</b>	Veronika Bartošová Faculty of Science, Masaryk University Department of theoretical physics and astrophysics
<b>Title of Thesis:</b>	Study of orientation evolution and passive attitude control of CubeSats
<b>Degree Programme:</b>	Physics
<b>Field of Study:</b>	Astrophysics
<b>Supervisor:</b>	Mgr. Filip Münz, PhD.
<b>Academic Year:</b>	2019/2022
<b>Number of Pages:</b>	xv + 50
<b>Keywords:</b>	attitude determination, GRBA $\alpha$ , nanosatellite, passive stabilization, sensors





# Abstrakt

Tato práce se zabývá zpracováním dat z nanosatelitu GRBA $\alpha$ , na jehož základě se snažíme vyvinout spolehlivou metodu určování orientace tohoto CubeSatu. V teoretické části jsme popsali příslušné souřadnicové systémy, které jsme následně použili i v praktické části. Představili jsme také základní technologie pro určování orientace a její kontrolu. V praktické části jsme použili informace ze slunečních senzorů a magnetometrů pro metodu TRIAD k co nejpřesnějšímu určení polohy družice.

# Abstract

This thesis deals with the processing of data from the GRBA $\alpha$  nanosatellite, on the basis of which we try to develop a reliable method of determining the orientation of this CubeSat. In the theoretical part we described the relevant coordinate systems, which we also used in the practical part. We have also introduced basic technology for attitude determination and attitude control. In the practical part we used information from sun sensors and magnetometers for TRIAD method to estimate the attitude of the satellite as accurately as possible.



ZADÁNÍ  
BAKALÁŘSKÉ PRÁCE

Akademický rok: 2021/2022

Ústav:	Ústav teoretické fyziky a astrofyziky
Studentka:	Veronika Bartošová
Program:	Fyzika
Specializace:	Astrofyzika

Ředitel ústavu PŘF MU Vám ve smyslu Studijního a zkušebního řádu MU určuje bakalářskou práci s názvem:

Název práce:	Study of orientation evolution and passive attitude control of CubeSats
Název práce anglicky:	Study of orientation evolution and passive attitude control of CubeSats
Jazyk závěrečné práce:	angličtina

**Oficiální zadání:**

GRBAAlpha, 1U CubeSat launched in March 2021, is a prototype of a new family of gamma-ray detectors intended for transient source monitoring and localization (triangulation method profiting of a precise timing). Satellite is equipped with a wide set of magnetometers, sun sensors and additional devices providing complex information about the satellite movement. Extracting exact attitude from this data is not a straightforward task. Moreover this movement is complicated by a system of permanent magnets fixed on the satellite that provide a passive attitude control, trying to align it with Earth magnetic field.

Student will develop a reliable method for determining nanosatellite orientation (using sensor data as well as knowledge of satellite position). The work might lead to a full model of satellite motion so even periods of scarce sensor readings could be used to improve precision of the attitude knowledge. The signal recorded by primary payload, the gamma-ray detector, sometimes also shows periodic signal related to satellite movement – this should be also studied in view of its sensitivity dependence on direction of incoming radiation. The data obtained from a sister CubeSat VZLUSat-2, that features identical gamma-ray detectors and is scheduled to be launched in the beginning of 2022, will help to clarify these orientation-related effects.

**Literatura:**

WERNER, Norbert, J. RIPA, A. PAL, M. OHNO, N. TARCAI, K. TORIGOE, K. TANAKA, N. UCHIDA, L. MESZAROS, G. GALGOCZI, Y. FUKAZAWA, T. MIZUNO, H. TAKAHASHI, K. NAKAZAWA, Z. VARHEGYI, T. ENOTO, H. ODAKA, Y. ICHINOHE, Z. FREI a L. KISS. CAMELOT: Cubesats Applied for MEasuring and LOcalising Transients - Mission Overview. In DenHerder, JWA; Nikzad, S; Nakazawa, K. *SPACE TELESCOPES AND INSTRUMENTATION 2018: ULTRAVIOLET TO GAMMA RAY*. BELLINGHAM: SPIE-INT SOC OPTICAL ENGINEERING, 2018. s. 1-15. ISBN 978-1-5106-1951-7. doi:10.1117/12.2313764.

OHNO, Masanori, Norbert WERNER, Andras PAL, Jakub RIPA, Gabor GALGOCZI, Norbert TARCAI, Zsolt VARHEGYI, Yasushi FUKAZAWA, Tsunefumi MIZUNO, Hiromitsu TAKAHASHI, Koji TANAKA, Nagomi UCHIDA, Kento TORIGOE, Kazuhiro NAKAZAWA, Teruaki ENOTO, Hirokazu ODAKA, Yuto ICHINOHE, Zsolt FREI a Laszo KISS. CAMELOT: design and performance verification of the detector concept and localization capability. In DenHerder, JWA Nikzad, S Nakazawa, K. *SPACE TELESCOPES AND INSTRUMENTATION 2018: ULTRAVIOLET TO GAMMA RAY*. BELLINGHAM: SPIE-INT SOC OPTICAL ENGINEERING, 2018. s. 1-12. ISBN 978-1-5106-1952-4. doi:10.1117/12.2313228.

PÁL, András, Masanori OHNO, László MÉSZÁROS, Norbert WERNER, Jakub ŘÍPA, Marcel FRAJT, Naoyoshi HIRADE, Ján HUDEC, Jakub KAPUŠ, Martin KOLEDA, Robert LASZLO, Pavol LIPOVSKÝ, Hiroto MATAKE, Miroslav ŠMELKO, Nagomi UCHIDA, Balázs CSÁK, Teruaki ENOTO, Zsolt FREI, Yasushi FUKAZAWA, Gábor GALGÓCZI, Kengo HIROSE, Syohei HISADOMIHI, Yuto ICHINOHE, László L. KISS, Tsunefumi MIZUNO, Kazuhiro NAKAZAWA, Hirokazu ODAKA, Hiromitsu TAKAHASHI a Kento TORIGOE. GRBA $\alpha$ : a 1U CubeSat mission for validating timing-based gamma-ray burst localization. In Jan-Willem A. den Herder, Shouleh Nikzad, Kazuhiro Nakazawa. *Proc. SPIE 11444, Space Telescopes and Instrumentation 2020: Ultraviolet to Gamma Ray, 114444V*. Bellingham: Society of Photo-Optical Instrumentation Engineers (SPIE), 2020. s. "114444V-1"- "114444V-10", 10 s. ISBN 978-1-5106-3675-0. doi:10.1117/12.2561351.

---

**Vedoucí práce:** Mgr. Filip Münz, PhD.

---

**Konzultant:** RNDr. Jakub Řípa, Ph.D.

---

**Datum zadání práce:** 22. 11. 2021

---

**V Brně dne:** 7. 5. 2022

---

Zadání bylo schváleno prostřednictvím IS MU.

Veronika Bartošová, 12. 1. 2022

Mgr. Filip Münz, PhD., 14. 1. 2022

prof. Mgr. Dominik Munzar, Dr., 14. 1. 2022

# Poděkování

Touto cestou sa chcem poďakovať svojmu vedúcemu Mgr. Filipovi Münzovi, Ph.D. za nekonečnú trpezlivosť, ktorú so mnou mal, každú radu, čo mi dal, a hodiny času, ktoré mi venoval. Ďalej sa chcem poďakovať svojmu konzultantovi RNDr. Jakubovi Řípovi, Ph.D. za jeho rady a v poslednom rade svojim rodičom a Lukášovi za ich podporu.

# Prohlášení

Prohlašuji, že jsem svoji bakalářskou práci vypracovala samostatně pod vedením vedoucího práce s využitím informačních zdrojů, které jsou v práci citovány

Brno 17. května 2022

.....  
Veronika Bartošová



# Contents

<b>Acronyms used</b> .....	<b>xv</b>
<b>Introduction</b> .....	<b>1</b>
<b>Chapter 1. Coordinate systems and reference frames</b> .....	<b>2</b>
1.1 Heliocentric-Ecliptic .....	2
1.2 Earth-Centered Inertial (ECI) .....	2
1.3 Earth-Centered Earth-Fixed (ECEF) .....	3
1.4 North East Down (NED) .....	3
1.5 Earth-centered orbit reference frame (OC) .....	4
1.6 Orbit reference frame (O) .....	4
<b>Chapter 2. Attitude determination</b> .....	<b>6</b>
2.1 Magnetometers .....	6
2.2 Sun sensors .....	7
2.3 Gyroscopes .....	7
2.4 Star trackers .....	7
2.5 Earth sensors .....	8
<b>Chapter 3. Attitude control</b> .....	<b>9</b>
3.1 Spin stabilization .....	9
3.2 Three-axis stabilisation .....	9
3.2.1 Wheels .....	10
3.2.2 Magnetic control torques .....	10
3.2.3 Thrusters .....	10
3.3 Passive control .....	11
3.3.1 Gravity gradient .....	11
3.3.2 Passive magnetic control .....	11
<b>Chapter 4. Data processing</b> .....	<b>12</b>
4.1 Data .....	12
4.2 Obtained data display .....	12
4.3 Satellite orientation .....	16
4.4 Rotating model vs. reality .....	22
4.5 Upgraded model .....	26

4.6 Third model . . . . .	29
4.7 Computed attitude . . . . .	31
<b>Conclusion . . . . .</b>	<b>34</b>
<b>Bibliography . . . . .</b>	<b>36</b>
<b>Appendix A . . . . .</b>	<b>39</b>
<b>Appendix B . . . . .</b>	<b>48</b>



# Acronyms used

ADCS	Attitude Determination and Control System
AOCS	Attitude Orientation Control System
COTS	Commercial Off-The-Shelf
CSACS	CubeSat Attitude Control Simulator
GRB	Gamma-Ray Burst
IMU	Inertial Measurement Unit
IRES	International Earth Rotation Service
LEO	Low Earth Orbit
MPPC	Multipixel Photon Current
MW	Momentum Wheels
OBC	On Board Computer
RW	Reaction Wheels
SSO	Sun-Synchronous Orbit
SXD	Space X-ray Detector
TLE	Two-line Elements
UHF	Ultra High Frequencies
VHF	Very High Frequencies
VZLÚ	Czech aerospace research centre (Výzkumný a zkušební letecký ústav, a.s)
WGS	World Geodetic System

# Introduction

In the past, launching satellites was not an easy task. Long series of performance tests were required before acceptance and even completed satellites often waited for years until convenient launch opportunity was found. This changed with CubeSats. Many of these have launched not only for academic purposes, but also for commercial and amateur projects. Their probably greatest advantage is that students can now see results of their work while they are still studying.

On 22<sup>nd</sup> of March 2021, small CubeSat, GRBAAlpha, was launched from Baikonur in Kazakhstan on the Soyuz-2 launch vehicle. It is a Low Earth Orbit (LEO) satellite whose mission is to prove the concept to detect gamma-ray bursts, extremely powerfull explosions in the Universe, with such a small device ([Pál et al. 2020](#)).

However, for a satellite to work properly, it must be able to detect where it is located and how it is oriented. Regardless of the mission, the more precise attitude determination is, the more accurate results we can get. Therefore, our goal was to develop a reliable method of determining the orientation of GRBAAlpha using data from its sensors – namely sun sensors and magnetometers.

The first three chapters of this thesis present a theoretical framework in which we introduce the most relevant coordinate systems as well as information about equipment necessary for attitude determination and attitude control. This segment of the thesis is followed by description of our research procedure and results we got.

# Chapter 1

## Coordinate systems and reference frames

In order to work properly spacecraft needs to be able to figure out where it is located and where it is pointing. Compared to devices on Earth surface, in space there are no fixed reference points.

For accurate description of orbital motion, we need to understand which coordinate system is used. The coordinate systems can be inertial, so that the frame is fixed to a remote observer. A coordinate system fixed to a moving body can be used to describe satellite motion as well. However a rotation between the inertial and Earth-fixed coordinate systems must be incorporated into the definition ([Makovec 2001](#), p. 45). ECEF is shown in Figure [1.1](#).

### 1.1 Heliocentric-Ecliptic

Bodies orbiting around the Sun, for example Earth, other planets and even interplanetary space vehicles, are best described in Heliocentric-ecliptic frame of reference. In Heliocentric-ecliptic coordinates the origin is the Sun center. Plane of references is the ecliptic plane, and the vernal equinox is the primary direction which corresponds with X-axis. Y-axis is specified to the west on the plane. Finally the Z-axis is pointing toward the north ecliptic pole ([Makovec 2001](#), p. 46).

### 1.2 Earth-Centered Inertial (ECI)

The Earth-Centered Inertial (ECI) coordinate system has its center in the middle of the Earth. Z-axis is defined as Earth rotation axis at epoch J2000. X-axis represents direction of the vernal equinox with Y-axis that is defined to create an orthogonal basis ([Finance et al. 2021](#), p. 6-7). The reference frame is shown in Figure [1.2](#) in blue.

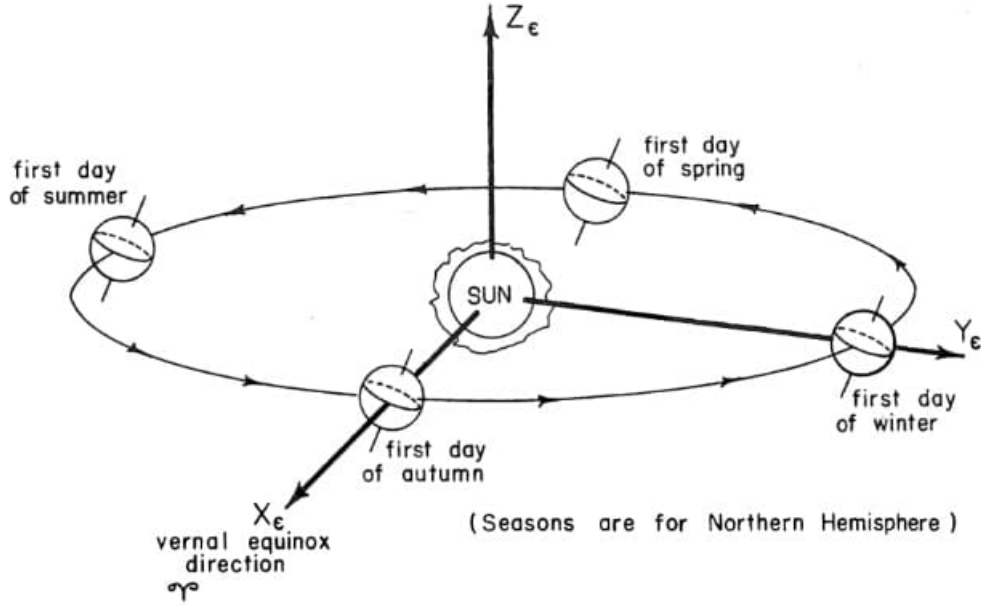


Figure 1.1: Heliocentric-ecliptic coordinate system (Bate et al. 1971).

### 1.3 Earth-Centered Earth-Fixed (ECEF)

The Earth-Centered Earth-Fixed (ECEF) coordinate system has its center also in the middle of the Earth. Z-axis passes through the North pole (International reference pole), as it is defined by the International Earth Rotation Service (IERS) (Snay et al. 1999, p. 32). X-axis represents direction to the Greenwich Meridian. The angle between the Greenwich Meridian and the vernal equinox direction is known as the Greenwich sidereal time,  $\theta$ . Greenwich sidereal time can be extracted from data tables as  $\theta_{g0}$ . At any time after epoch,  $\theta$  can be determined from  $\theta_{g0}$  by

$$\theta = \theta_{g0} + \omega_{\oplus}(t - t_0), \quad (1.1)$$

where  $\omega_{\oplus}$  is the angular velocity of the Earth. Y-axis is defined to make reference frame into an orthogonal basis. The reference frame is shown in Figure 1.2 in red (Finance et al. 2021, p. 7).

### 1.4 North East Down (NED)

Let's suppose a WGS 84 (World Geodetic System) is ellipsoid model of the Earth. The North East Down (NED) is a local reference frame that moves the body frame's position in the ECEF. It is defined by local tangent plane coordinates, which means, that the X–Y plane is tangential to the surface of the ellipsoid at the given location in the ECEF. Based on these conditions, the X-axis is pointing toward true North, the Z-axis is pointing to the Earth's center. Finally the Y-axis completes the orthogonal base. Shown in Figure 1.2 in purple (Finance et al. 2021, p. 7).

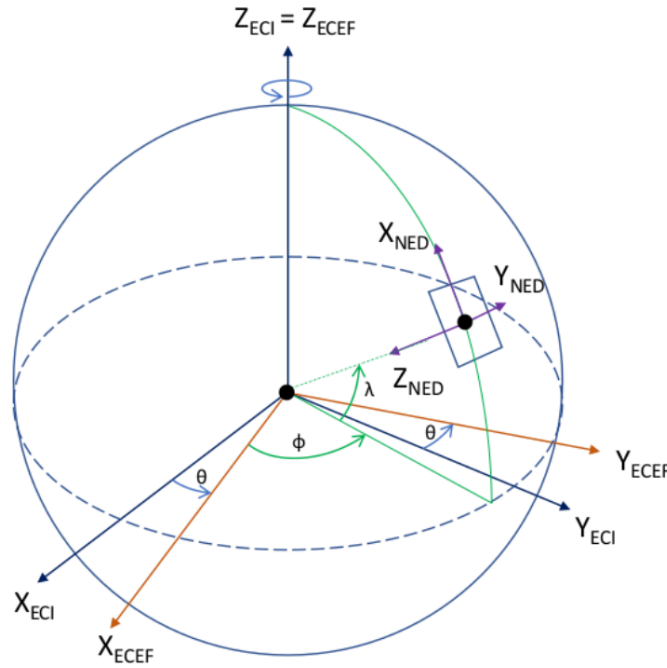


Figure 1.2: (Earth-Centered Inertial (ECI), Earth-Centered Earth-Fixed (ECEF), North East Down (NED)). (Finance et al. 2021).

## 1.5 Earth-centered orbit reference frame (OC)

Body orientation in an orbit is described by attitude dynamics. It can also be parameterized using rotations. For examining attitude evolution it is necessary to find a suitable reference frames to be used as base for the rotation (Makovec 2001, p. 63).

The reference frame is centered at the Earth's center, with the X-axis towards the perigee, the Y-axis along the semi-minor axis, and the Z-axis perpendicular to the orbital plane to complete the right-hand system. We need to define frame of reference of which origin coincides with the center of the satellite (Finance et al. 2021, p. 7). The reference frame is defined in Figure 1.3.

## 1.6 Orbit reference frame (O)

Orbit reference frame is defined with its origin located in the center of satellite. The origin rotates with an angular velocity of  $\omega_0$  relative to the ECI. Axes X, Y, Z create right-hand system, where Z-axis aims towards the middle of the Earth, X-axis is pointing in spacecraft's direction of motion while perpendicular to Z-axis and Y-axis complements the system (Finance et al. 2021, p. 7).

Sun-synchronous orbit (SSO) is fixed to the Sun. Orbital plane of geocentric satellite must rotate around the Sun with angular velocity of 1 degree per day, what is approximately an angular velocity of the Earth. This type of orbit makes the satellite keep the angle of sunlight on the surface of the Earth as consistent as possible (Riebeek 2009).

However, the orbit reference frame of GRBAIpha is not fixed to stars, nor the Earth and neither to the Sun. As it orbits the Earth, it revolves around the Sun. It has a polar orbit, so it is subject to orbital precession, as shown in Figure 1.4.

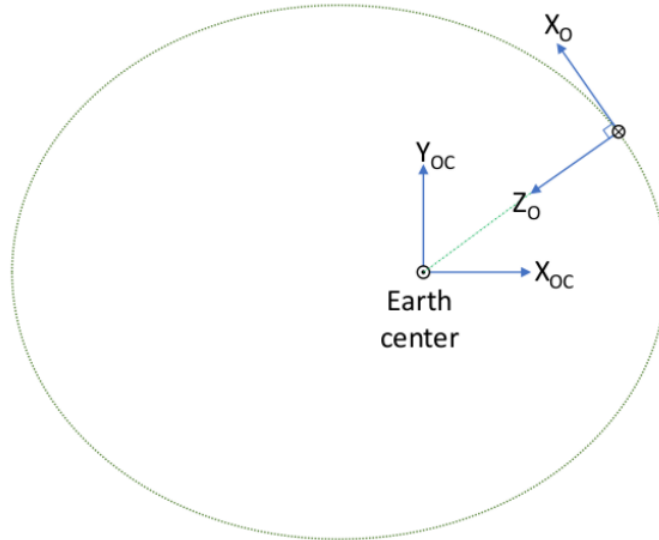


Figure 1.3: Earth-centered orbit reference frame and orbit reference frame (Finance et al. 2021).

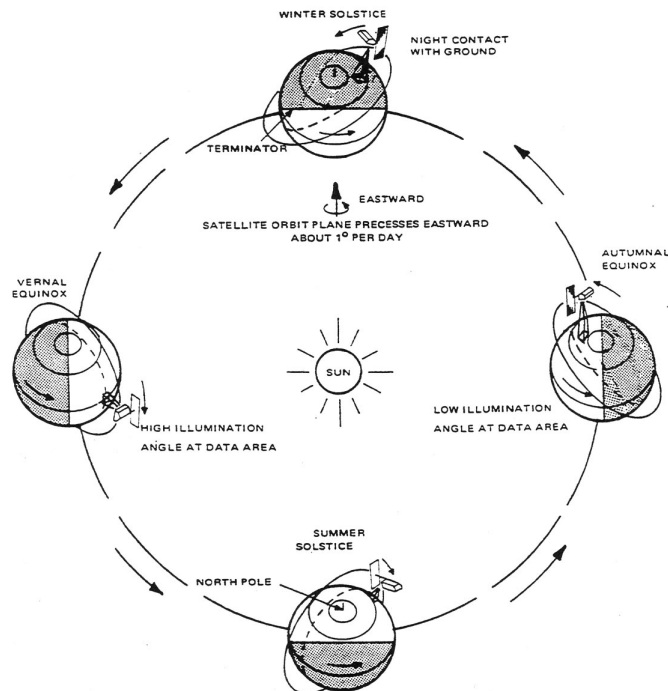


Figure 1.4: Orbital precession ( [online](http://tornado.sfsu.edu/Geosciences/classes/m415.715/MonteVerdi/Satellite/seasons.jpg)<sup>1</sup>).

<sup>1</sup>Online: <http://tornado.sfsu.edu/Geosciences/classes/m415.715/MonteVerdi/Satellite/seasons.jpg>

# Chapter 2

## Attitude determination

### 2.1 Magnetometers

Magnetometers are sensors measuring strength of magnetic field in single direction. By combining three orthogonal magnetometers, we will get 3-axis magnetometer, that measures not one, but three components of the magnetic field. It is used to measure geomagnetic field vector and to determine attitude of satellites. Measurements are corrupted by noise, that can be made up of biases, scale factor errors, alignment errors or electrical activity of spacecraft. However, the greatest effect on the noise emerges from the magnetic field model. For near Earth orbits, the type of orbit plays a major role in the magnetic field model. Near the equator, the modelled field direction error can vary from 0.5". Near the magnetic poles, where auroral electric currents play a significant role, the modelled field direction error can vary from 3" (Shuster et al. 2005, p. 258).

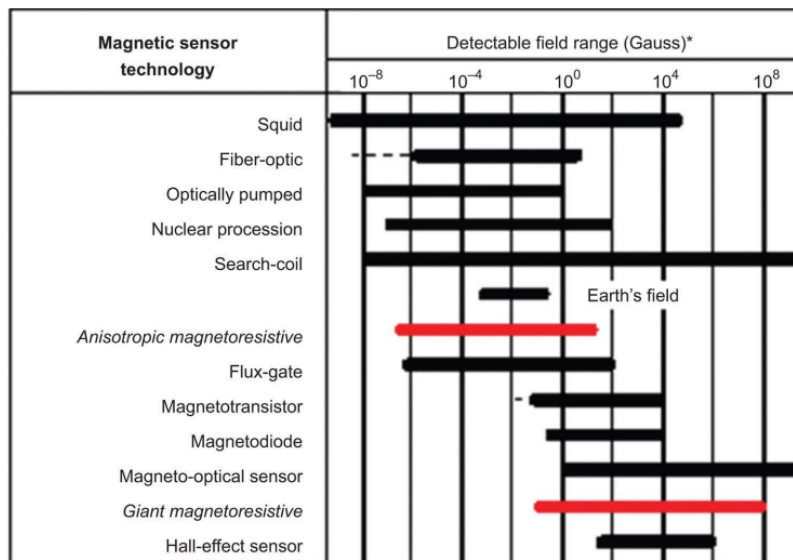


Figure 2.1: Sensitivity ranges of different types of magnetometers (Zheng 2017).

Based on strength of magnetic fields, we can classify it into three types: weak magnetic field (<1 mG), medium magnetic field (1 mG–10 G), strong magnetic field (>10 G).

Similar to magnetic fields, we can establish three types of magnetometers, based on their sensitivity: high-sensitivity magnetometers, medium-sensitivity magnetometers and low-sensitivity magnetometers ([Zheng 2017](#), ch. 9).

## 2.2 Sun sensors

Sun sensors are part of the satellite navigation system. These sensors determine the relative orientation of the Sun and the satellite. They provide satellite orientation data using solar vector altitude and azimuth. Third component of the vector is needed to completely determine position of the satellite, which we can detect using another sensor, for instance a magnetometer or an earth sensor. The disadvantage of sun sensors is the fact that we do not always see the Sun. At the time of the eclipse in the orbit, the sensor is essentially non-functional. We can use to a certain degree solar panels as an alternative to sun sensors to determine the direction of the Sun (we do this by detecting changes in current) ([Sumathi et al. 2013](#)).

When choosing a sun sensor, we take into account its size and accuracy. For CubeSats, nonetheless, we can accommodate only smaller sun sensors that are relatively inaccurate. Because of this we rely mostly on magnetometer data as primary vector, using sun sensors as complementary information.

There are three main technological categories of sun sensors:

1. **Coarse analog solar sensors:** measure the current output, which is proportional to the cosine of the angle between the sun and the photocell normal.
2. **Fine analog solar sensors:** use an aperture to create a sunspot, either on a four-quadrant photodiode or on a position-sensitive device.
3. **Digital solar sensors:** which operate by integrating a 2-dimensional light sensor and signal processing to distinguish between direct solar radiation and reflected solar radiation (mostly from the Earth's surface) ([Hywel 2020](#)).

## 2.3 Gyroscopes

Gyroscopes are devices that measure the speed of rotation of a satellite. They are located inside the satellite and operate at every point in orbit. Their advantage is good accuracy, but only for restricted time intervals. The drawback is that they only measure the change of position, not the position itself ([Makovec 2001](#), p. 56).

## 2.4 Star trackers

A star tracker is a navigation tool that is used, among other things, to determine the orientation of a host satellite (it scans stellar constellations and selects known stars that are compared with data in the satellite's catalog) ([Makovec 2001](#), p. 56). Usually 50 to 60



navigation stars are used to determine the position of a satellite. On-board systems then process the images and determine the orientation of the satellite in its reference frame.

Great advantage of star trackers is their accuracy. Moreover, they work in any point in an orbit. The star tracker must take into account the interference effects of light reflected from the satellite's surface. The high level of radiation from which the cameras must be protected is also a problem. For small satellites, their weight is also important. Many satellites currently involve a lot of commercial off-the-shelf (COTS) type of star trackers. That is why, when choosing a star tracker (and all other components), mutual interoperability and assembly of devices must be taken into account (Hywel 2019).

## 2.5 Earth sensors

Earth sensors have important role in attitude determination of a satellite (pitch axis and roll axis). In this case, the advantage is the size and brightness of the Earth, which is impossible to confuse with other body (Zafar et al. 2019).

The principle of determining the orientation of a satellite is based on determining the position of the Earth, especially the horizon line. There are two types of earth horizon sensors: static and scanning. Static horizon sensors (Figure 2.2) contain several sensors sensitive to infrared radiation from Earth's surface. Their field of view is slightly larger than the Earth. The signal from each sensing element is proportional to the fraction of its field of view on which the Earth intrudes. Some disadvantage is the low resolution of only  $0.1^\circ$  (due to an uncertainty in the horizon). Principle of earth horizon scanners is more complex and consequently more expensive. It employs a spinning prism or mirror and other components shown in Figure 2.3. The scanning motion is needed, because it needs to cover a larger segment of space than its primary field of view enables (Shuster et al. 2005, p. 261-263).

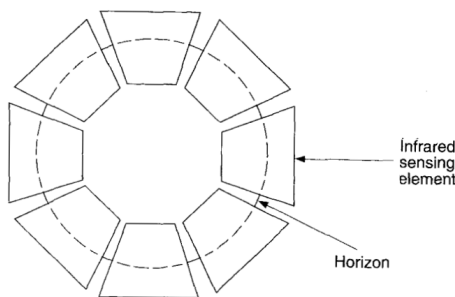


Figure 2.2: Static earth horizon sensor (Shuster et al. 2005, p. 262).

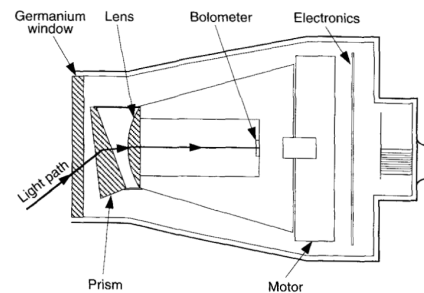


Figure 2.3: Scanning earth horizon sensor (Shuster et al. 2005, p. 263).

# Chapter 3

## Attitude control

To change the attitude of a spacecraft or to keep it in a defined orientation, some form of attitude control is needed. In following chapter we will introduce three ways of an attitude control, namely spin stabilization, three-axial control technique, and passive control (Makovec 2001, p. 56)

### 3.1 Spin stabilization

Satellites are usually spin-stabilised during the orbital manoeuvring phase, and a lot of them use the spin effect at some point in their lifetime. As a general rule, a body rotating about its major or minor axis keeps the direction of its axis of rotation fixed with respect to an inertial frame. According to Euler's equations of motion, this direction changes only if external moments act about its center of gravity and perpendicular to the axis of rotation (Sidi 1997, p. 132).

Single-spin spacecrafts spin about the angular momentum vector. It is quite simple method, but downside is high angular momentum, which is the reason for poor maneuverability. Dual-spin spacecraft represents a more complex system, where majority of spacecraft is spun, but its payload section is rotating in the opposite direction about the same axis (Makovec 2001, p. 57)

Single-spin rotation is mainly used because of its simplicity and efficiency. Attitude control and stabilization of a spacecraft stabilized by single-spin rotation usually requires some measurements of angular velocity. However, two-spin stabilization is considerably better from a communication point of view (Sidi 1997, p. 144, 148).

### 3.2 Three-axis stabilisation

Three-axial systems have better pointing accuracy than spin stabilized. Better technology is however expensive, complicated and devices are bigger and heavier (Makovec 2001, p. 57).

### 3.2.1 Wheels

Thanks to reaction wheels and gyroscopes spacecrafts can change their orientation without using fuel. These devices operate on the principle of conservation of an angular momentum.

Reaction wheels and momentum wheels are near synonyms. Manufacturers usually do not distinguish between the two, since the same device can be used either as reaction wheels (RW) or momentum wheels (MW). So where lies the difference? The difference is in the use. Reaction wheels have nominal rotation rate close to zero. Its goal is to actively control rotation state of spacecraft. For small rotation rate, reaction wheels in orthogonal position are act nearly independently. Momentum wheels, on the other hand, have non-zero nominal rotation rate. Bigger rotation rate adds off-axis stability to spacecraft. Wheel's rotation axis, in both cases, is fixed with respect to spacecraft and angular momentum is transferred between spacecraft itself and the wheel by changing the wheel's rotation rate.

Another way of controlling spacecraft's attitude is by control moment gyros (CGMs). Their rotation rate has very high speed (much higher then RW or MW) and is nearly constant. As they operate at high rotation rates, the torque that results from a small orthogonal push can be very large. Rotating axis is not fixed with respect to spacecraft. These devices are much more complex and expensive then previous. They require precise manufacturing, controllers and sensors. They are used only on large spacecraft, such as International Space Station ([Hammen 2020](#)).

### 3.2.2 Magnetic control torques

Magnetic control devices use the interaction of the spacecraft magnetic dipole moment and the Earth's magnetic field to provide a control torque. However, electric currents and spurious magnetic effects can cause a disturbance torque. This detail needs to be taken into account when designing a spacecraft. Advantages of this type of attitude control are no fuel requirements and controllable torque magnitude. Some disadvantages are for example absence of torque about the local field direction and altitude and latitude torque sensitivity ([Fortescue et al. 2003](#), p. 301-302).

### 3.2.3 Thrusters

Thrusters provide the great source of force on spacecraft and the largest source of torque. Torque affects the total momentum of spacecraft. The thrust vector should pass through the center of mass, but in reality there are imperfections in spacecrafts, which arise disturbance torques.

Thrusters with a low level of thrust are commonly used in attitude control systems. For this purpose, they are mounted in clusters on the surface of spacecraft pointing in different directions. This way they can provide three components of torque. In comparison with magnetic torquer, their main advantage is the independence of their torquer of altitude and potentially there is no limit to its magnitude ([Fortescue et al. 2003](#), p. 299-301).

## 3.3 Passive control

### 3.3.1 Gravity gradient

Satellites can be stabilized in a nadir pointing attitude using gravity gradient phenomena. This nadir pointing stabilisation is acting in pitch and roll, but yaw is not controlled. The gravity gradient torque for satellites orbiting Earth is caused by differences in the distance to Earth across the satellite body. Some parts are closer to the Earth and their mass experiences higher gravitational pull. For cylindrical satellites, or 3U CubeSats, the length of satellites tends to line up with nadir ([Rawashed 2010](#), p. 12, 27, 28).

### 3.3.2 Passive magnetic control

Passive magnetic stabilization is made possible using a system of permanent magnets on board of the spacecraft. Function of passive magnetic stabilization is used mainly by LEO satellites on which the magnetic field has a greater influence than on medium or high orbit satellites. The permanent magnets make satellite to align with lines of the Earth's magnetic field during its orbit (it becomes something like a compass). This method is most effective for satellites with equatorial orbits, but it is also used by satellites with a polar orbit. In this case, the magnetically stabilized satellite would perform two cycles in orbit, where it would line up from north to south above the equator. The satellite must tumble above the Earth's magnetic poles to align with the Earth's magnetic dipole ([Rawashed 2010](#), p. 13).

# Chapter 4

## Data processing

### 4.1 Data

For this thesis we used set of data from GRBAAlpha from October 2021. It contains 300 seconds of observation time with 147 measured points. This set embraces several types of data. Information important for us is shown in Table 4.1.

Table 4.1: Indexes of relevant GRBAAlpha data.

Sensor	Direction	Unit
LdSt mag	X, Y, Z	nT
SolT	X $\pm$ , Y $\pm$ , Z-	°C
ssTemp	X $\pm$ , Y $\pm$ , Z-	°C
ssIRRad	X $\pm$ , Y $\pm$ , Z-	-
ssGyroX	X $\pm$ , Y $\pm$ , Z-	deg/s
ssGyroY	X $\pm$ , Y $\pm$ , Z-	deg/s

Details on individual sensors can be found in [Appendix A](#). The processes of communication and obtaining data from the satellite are in [Appendix B](#).

### 4.2 Obtained data display

The first step was to retrieve raw data from the satellite. Although we have data from five directions (from gyroscope), only three are shown in following figures for aesthetic purposes.

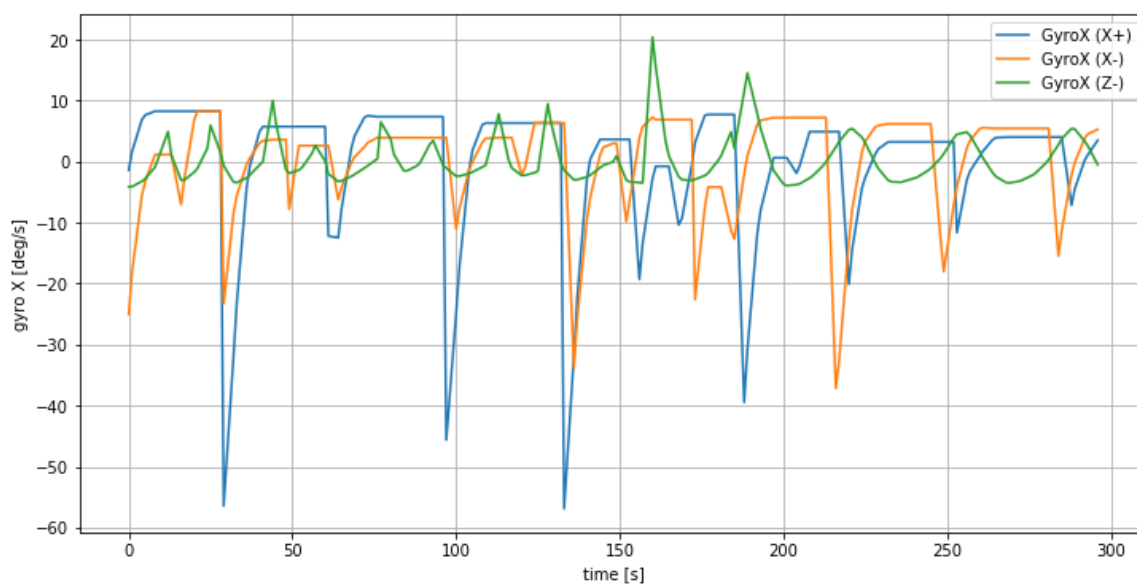


Figure 4.1: Data from gyro X.

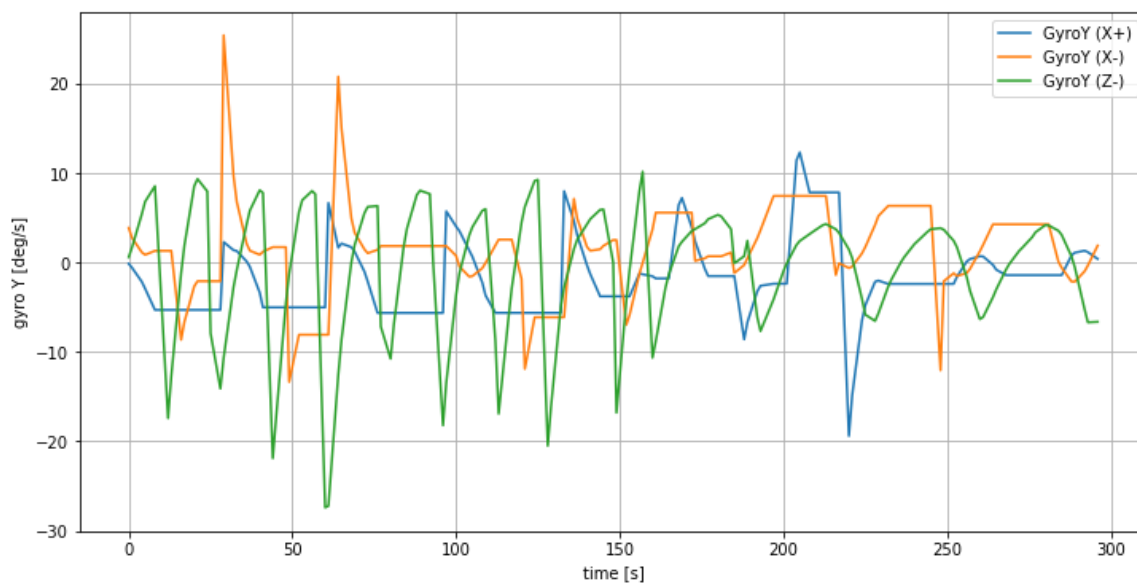


Figure 4.2: Data from gyro Y.

Then we took a look at temperature data from solar panels and sun sensors. From Figures 4.3 and 4.4 we can conclude that temperatures given by the sun sensors and solar panels at the same time more or less correspond. However, data from sun sensors are not applicable. Figure 4.4 shows digitization jumps. Temperature is rounded to 1 °C. On the other hand, the temperature measured by solar panels is determined to two decimal points, but we should doubt the accuracy in these ranges. Orientations of GRBAAlpha sun sensors are described in [Appendix A](#).

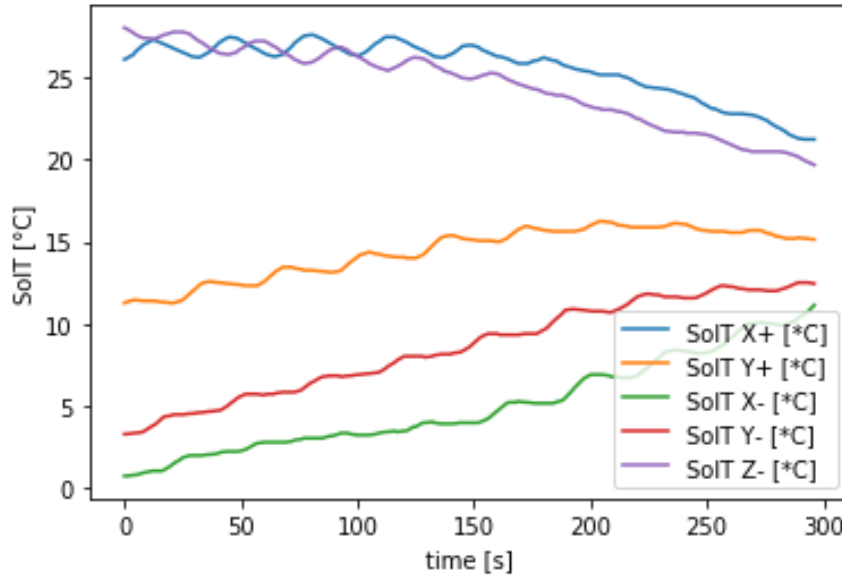


Figure 4.3: Data from solar panels (SolT).

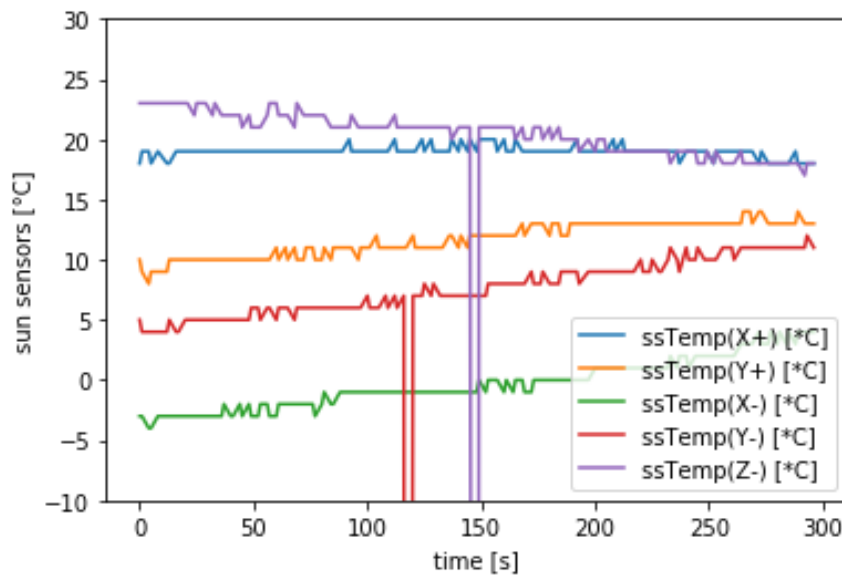


Figure 4.4: Data from sunsensors (ssTemp).

Last, but not least, we have data from magnetometer on Lodestone. Its time dependence is displayed in the Figure 4.5 below. If we look at the raw data sheet, we will see that the times between measurements are different. We have an irregular sampling, where a 1-second period and a 3-second period alternate.

By dividing the data from Figure 4.5 by time, we adjust angles by leaps that are caused by different measurement times. In Figure 4.6 are shown angles between two consecutive vectors divided by the time that has elapsed between them. From its shape we can deduce that the movement of the satellite is not completely regular and it wags in space. Naively we can imagine that GRBAAlpha is stabilized like a compass needle. More on that topic in section 3.3.2. After examining Figure 4.6 we can say, that its orientation to the north of magnetic field shifts by 4 to 6 degrees per second. The satellite is hence not fixed in the north direction, but it rotates or tumbles. This contradicts hypothesis, based on which we would consider the satellite being already stabilized or to be slowly drifting with respect to magnetic field.

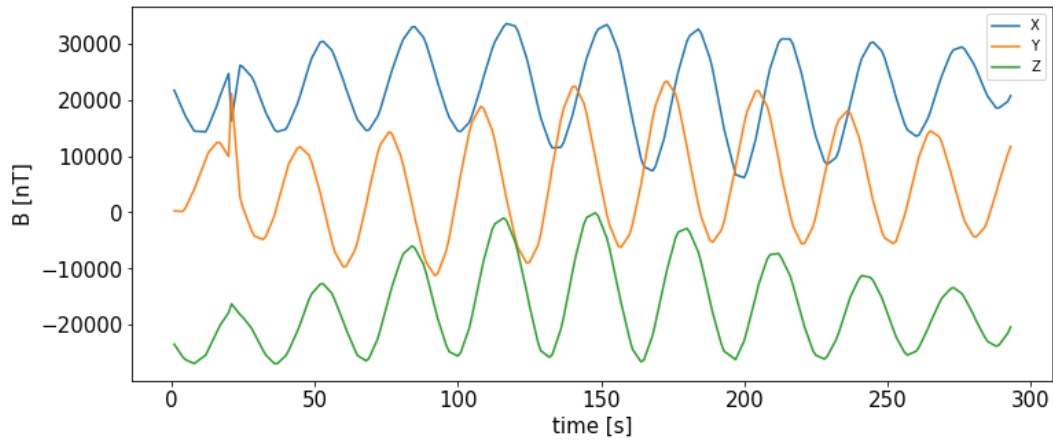


Figure 4.5: Data from magnetometer (LdSt mag).

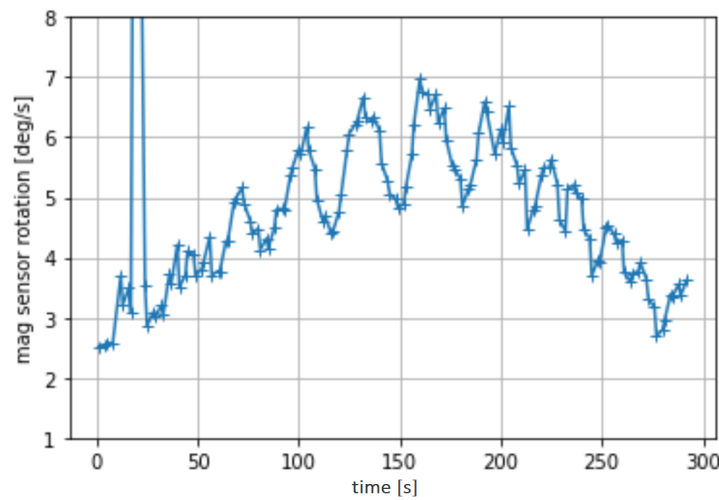


Figure 4.6: Adjusted data from magnetometers.



### 4.3 Satellite orientation

Attitude of a spacecraft can be determined using various methods, typically using formalism in a form of quaternions, Euler angles and a rotation matrix. For our purposes we chose Tri-Axial Attitude Determination method (TRIAD). The result of the TRIAD is a rotation matrix e.g. from orbit reference frame (O) to body reference frame (B) (reference frame of satellite). This is so-called Attitude Matrix. To compute the attitude matrix we need sun vectors and magnetic field vectors in both reference frames. Vectors in the body reference frame can be retrieved from on-board devices of GRBAAlpha. Vectors in the orbital reference frame are computed using model of magnetic field and celestial mechanic for the Sun position. When in eclipse, nadir vector is used instead of sun vector. However, determining nadir from infrared sensors is more difficult and results are less accurate. In TRIAD, the most accurate vector should be used as the first axis. In our case the most accurate is magnetic field vector. The direction to the Sun measured on board is not reliable as we would like it to be. Besides we are also missing sensor on Z+ side, where gamma-ray detector is placed. If we have a pair of vectors and we want to calculate the third one, which is perpendicular to them, we use the vector product as shown in equations 4.1 and 4.2,

$$\vec{t}_{1B} = \frac{\vec{b}_B}{\|\vec{b}_B\|}, \quad \vec{t}_{2B} = \frac{\vec{b}_B \times \vec{s}_B}{\|\vec{b}_B \times \vec{s}_B\|}, \quad \vec{t}_{3B} = \vec{t}_{1B} \times \vec{t}_{2B}, \quad (4.1)$$

$$\vec{t}_{1O} = \frac{\vec{b}_O}{\|\vec{b}_O\|}, \quad \vec{t}_{2O} = \frac{\vec{b}_O \times \vec{s}_O}{\|\vec{b}_O \times \vec{s}_O\|}, \quad \vec{t}_{3O} = \vec{t}_{1O} \times \vec{t}_{2O}, \quad (4.2)$$

where  $\vec{b}$  represents magnetic vector and  $\vec{s}$  represents sun vector. Vectors  $\vec{b}_B, \vec{s}_B$  are in the body frame (retrieved from GRBAAlpha). Then the TRIAD's basis can be expressed as a 3x3 matrix  $M_B = \{\vec{t}_{1B}, \vec{t}_{2B}, \vec{t}_{3B}\}$  in the body frame. Vectors  $\vec{s}_O, \vec{b}_O$  are in orbital frame computed from models. Then 3x3 orbital matrix can be expressed as  $M_O = \{\vec{t}_{1O}, \vec{t}_{2O}, \vec{t}_{3O}\}$ . With this information, we can define rotation matrix (Attitude matrix)  $R_{TRIAD,O \rightarrow B}$  as

$$R_{TRIAD,O \rightarrow B} = M_O M_B^T. \quad (4.3)$$

TRIAD matrix is a mediator between orbital and body frame, based on magnetic field and sun vectors (Hall 2003, ch. 4). Visual expression of TRIAD frame in the body reference frame is shown in Figure 4.7. In our calculations, however, we use ECI instead of the orbital reference frame. The reason is practical – easier calculation of position of the Sun.

As a next step, we used [Celestrak](https://celestrak.com/)<sup>1</sup>, which provides (and updates) orbital parameters for a number of Earth-orbiting bodies. Celestrak draws data from [NORAD](https://www.norad.mil/)<sup>2</sup> US military service, which has also defined a description of orbital parameters. Satellite orbits are changing, so the data must be updated regularly. We used [General Perturbations \(GP\)](#)

<sup>1</sup>Online: <https://celestrak.com/>

<sup>2</sup>Online: <https://www.norad.mil/>

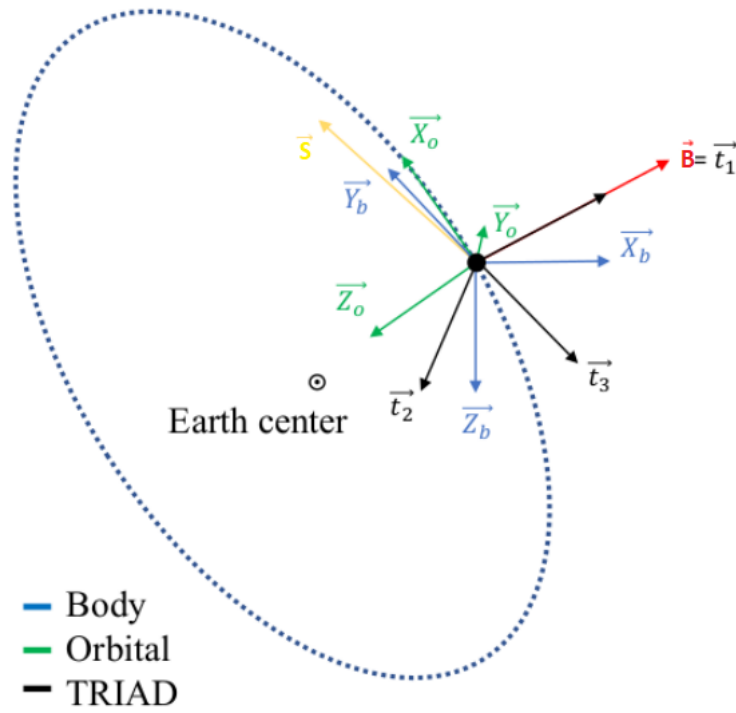


Figure 4.7: Reference frame for TRIAD ((Finance et al. 2021), modified for our requirements).

Element Sets<sup>3</sup>, data in two-line element set (TLE) format (a data format encoding a list of orbital elements of an Earth-orbiting object for a given point in time (Kelecy et al. 2007)). Ground stations use these data to calculate location of satellite during transmission. More about this process in Appendix B.

Specifically, we calculate longitude, latitude and real height during the measurement. It is also necessary to determine parameters of the Earth magnetic field, namely we obtain total intensity, declination, inclination, north intensity, east intensity, vertical intensity, horizontal intensity. From east, north and vertical intensities, we determine normalized magnetic field intensity vectors every position. We obtained this information from online calculator of British Geology Service [geomag.bgs](https://geomag.bgs.ac.uk/)<sup>4</sup>.

Using TLE data, we can make a GRBAAlpha motion model as demonstrated in Figure 4.8. Then we calculated (using the above-mentioned online service) the orientation of the magnetic vector during flight of the satellite – see Figure 4.9. We can use Figure 4.12 to better visualize the satellite's orbit (it moves from south to north). The red line represents the orbit that the satellite travelled while collecting our data. The purple line shows the path of several orbits. Its displacement is given by the rotation of the Earth (not by the precessive rotation of the plane of orbit at the SSO). We know that the intensity of the magnetic field is changing, as shown in Figure 4.10. Assuming the total magnetic intensity

<sup>3</sup>Online: <https://celestrak.org/NORAD/elements/>

<sup>4</sup>Online: [https://geomag.bgs.ac.uk/data\\_service/models\\_compass/wmm\\_calc.html](https://geomag.bgs.ac.uk/data_service/models_compass/wmm_calc.html)

should not vary fast (not periodically), we tried to reduce the apparent oscillations of the measured magnetic field by slightly adjusting calibration in individual axes. The result is shown in Figure 4.11: the blue line is the originally measured amplitude of the magnetic field vector, the yellow line is a result of our efforts to re-normalize the axes, in order to minimize above-mentioned oscillations of the magnetic field.

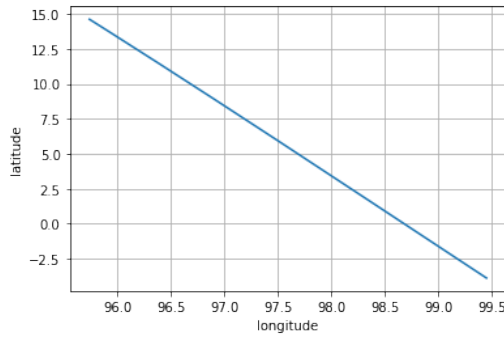


Figure 4.8: GRBAAlpha motion model from TLE data.

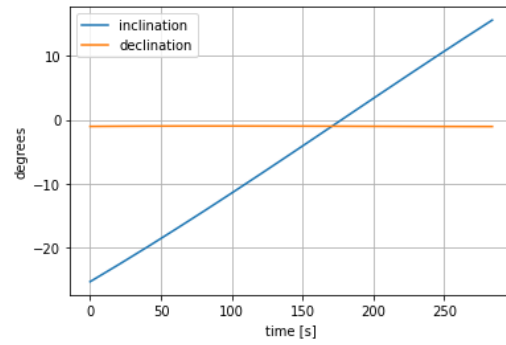


Figure 4.9: Orientation of the magnetic vector during flight of GRBAAlpha.

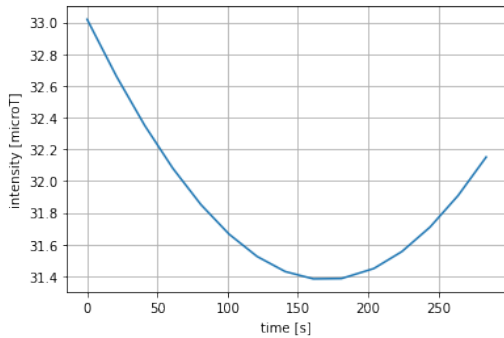


Figure 4.10: Development of magnetic field intensity.

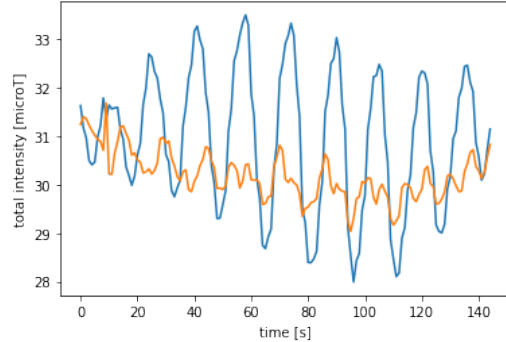


Figure 4.11: Total intensity of measured magnetic field.

After obtaining magnetic field vectors, sun vectors are needed. Again, we need data during satellite's recorded motion. From the `astropy.coordinates` package we used the `get_sun` function to get coordinates of the Sun's position, longitude and latitude. From this we calculated the direction to the Sun in ECI.

Concerning the data measured in the body frame, we assumed that the magnetometer on Lodestone module measures (after small renormalization) correctly. We fixed the magnetic field vector in the direction of magnetic north. All that remained was to determine the third angle. We calculated the angle between calculated magnetic vector and the vector towards the Sun (in ECI frame). As the satellite was moving, this angle was changing. Then we simulated Sun direction in body coordinate frame (satellite coordinate frame) for all possible rotations perpendicular to magnetic field. Our goal was to find a set of vectors

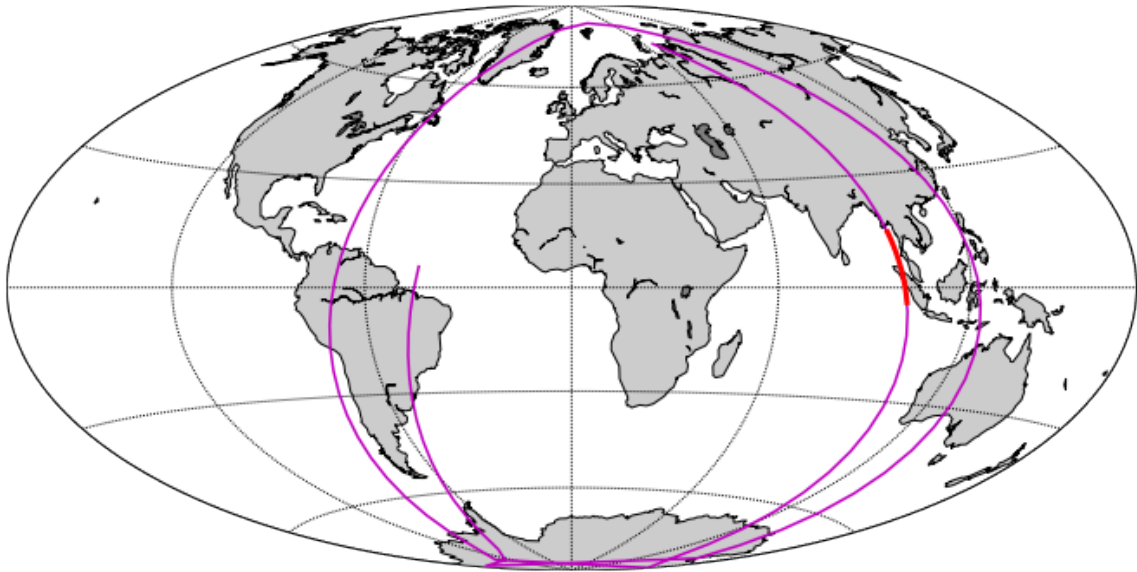


Figure 4.12: GRBA Alpha's orbit. The red line represents the part of the orbit we are studying.

that have the same angle. In Figure 4.13 an example of what sun direction component in satellite body frame looks like, when Sun rotates in a plane perpendicular to the magnetic field, is shown.

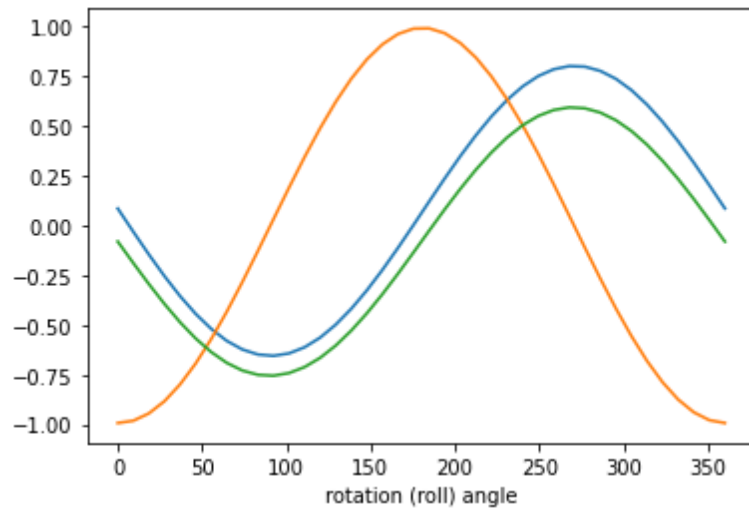


Figure 4.13: Sun direction components in satellite body frame.

Before importing data from sun sensors (ssIRRad), we tried to calibrate it. We downloaded as much available data as possible from the beginning of the GRBAAlpha campaign (usually sparse measurements from logfiles) and created histograms shown in Figures 4.14, 4.15 and 4.16. Histograms are given in absolute values. For further analysis we used only values greater than 7000, below which we observe secondary maxima that should correspond to the light reflected from the Earth (see Figure 4.17). Histograms bellow show three types of information. The first information is that sensors most frequently detected nothing – the first and highest column of the histograms. A few higher columns next to it correspond to the albedo from the Earth, which also comes commonly into the field of view of the sun sensors. We see that it really is a significant source of light. Remaining lower columns to the right of this region represent signal from the Sun. From this part of the histograms we omitted the upper and lower 10% of the data: this step made the scale of the range we measure more robust. Our aim is to use this information to correct our models so that sensitivity of sun sensors is equal for all 5 directions (Figure 4.14). Corrected data are shown in Figure 4.18.

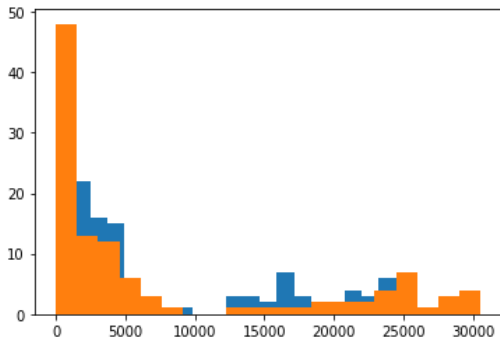


Figure 4.14: Histogram for X-axis (both + and -) sun sensor.

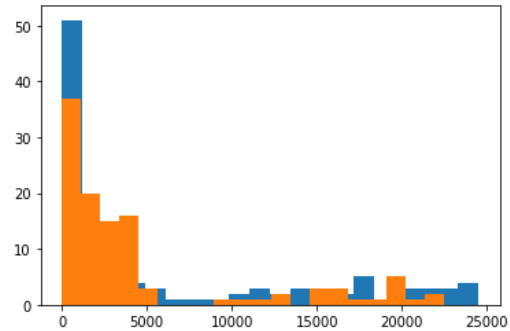


Figure 4.15: Histogram for Y-axis.

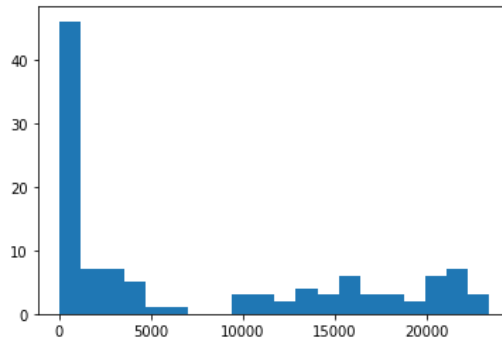


Figure 4.16: Histogram for Z-axis.

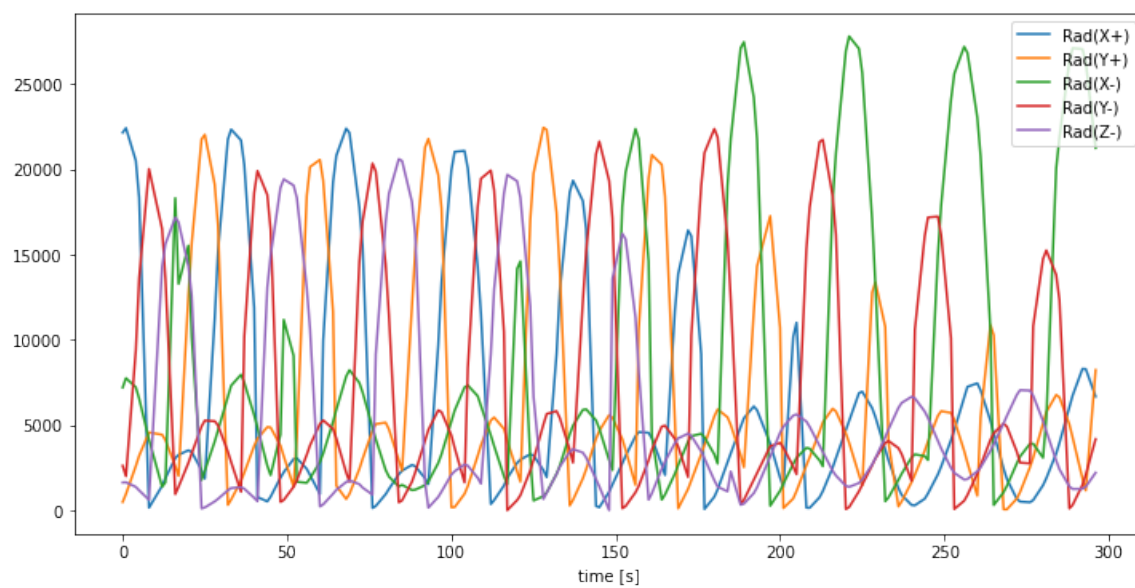


Figure 4.17: Development of illumination of sun sensors in five axes.

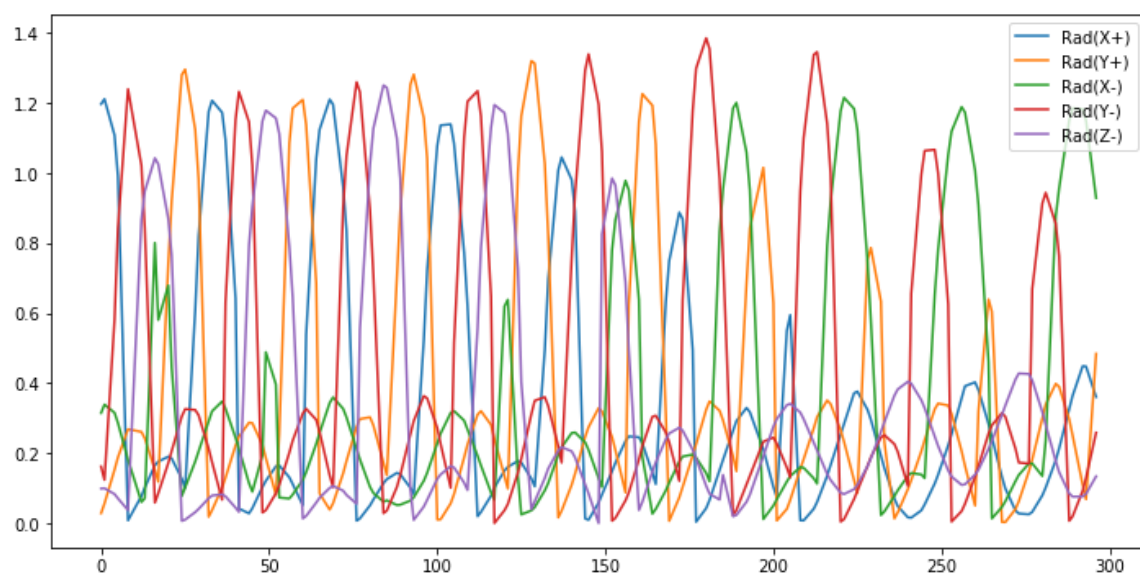


Figure 4.18: Corrected data from sun sensors (ssIRRad).

## 4.4 Rotating model vs. reality

In this section, we tried to find a description of the motion where the predictions best correspond to observations. Because of some remaining uncertainty about the normalization of the sun sensor data, correlation coefficient was used to give a robust estimate of the match between the model and reality.

Figure 4.19 below shows an attempt to find such correlation comparing each direction of the model (simulation) with reality. We see that the only sensor where our model agrees with reality is the point (X+).

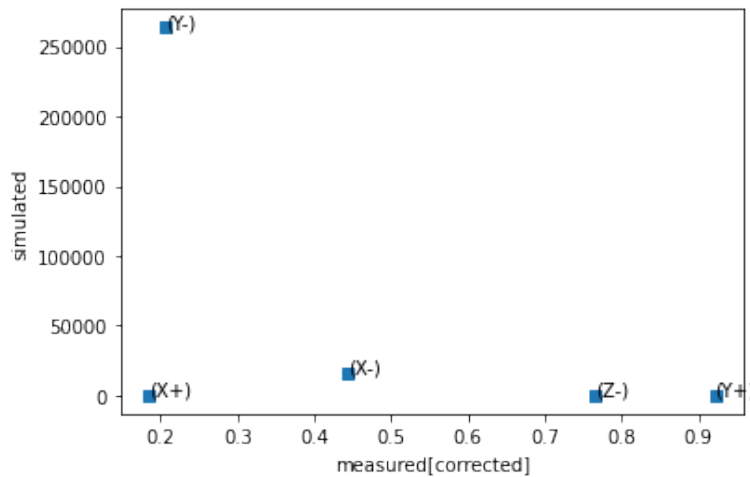


Figure 4.19: Correlation of model with real data.

The problem with this solution is its obvious inefficiency. Creating similar diagrams for each unit of measurement and every modelled orientation is unnecessary. A more efficient solution is to create a dynamic diagram as in Figure 4.20. With different rotations of the satellite in the direction perpendicular to the magnetic field we want to find out when there is the best match between the model and real data. For the given time we use only values whose correlation is better than 0.8. We're trying to find a match between the outputs from the sun sensors and the satellite's rotation. The problem is that we do not have a clear interpretation for sun sensor data, i.e. we cannot determine the direction of the Sun from it if it is within its field of view: we only know whether the sun sensor is oriented closer to the Sun or further.

As we look at Figure 4.20, we can see almost linear growing lines made of red triangles: this indicates a rotation. At the beginning, within about 180 seconds, we have a fairly good motion sketch. Then the graph begins to fall apart. The reason is probably the signal for (X-) coordinate (Figures 4.17, 4.18 - green line), which starts to appear at this time, and the good angles based on which we created our model fall into the background. More universal model should be developed, ideally with (Z+) sun sensor (but in case of GRBAAlpha it is not possible, since the entire (Z+) area is used for the GRB detector).

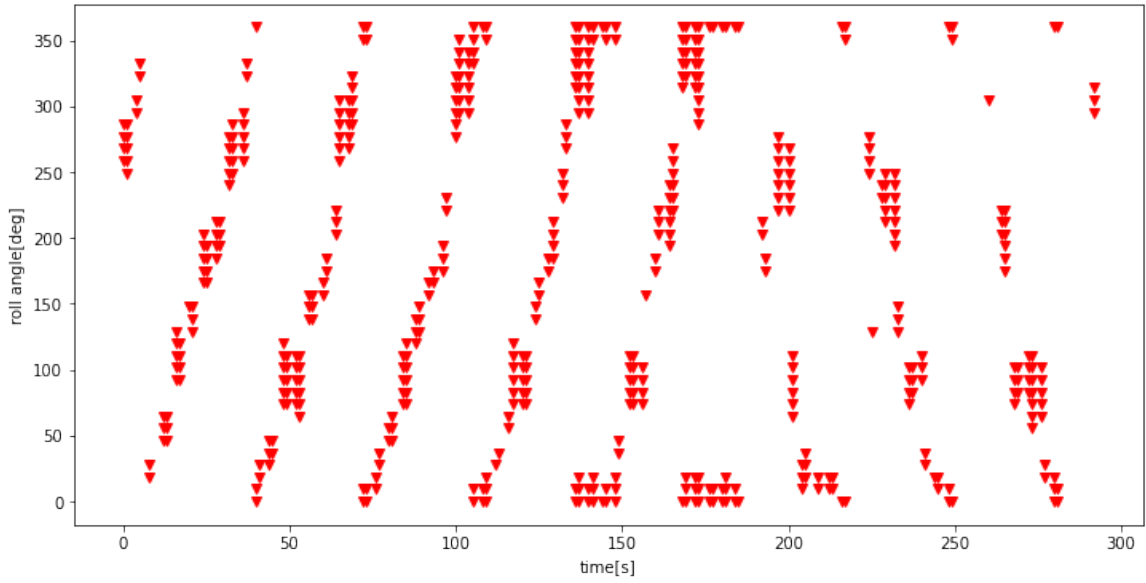


Figure 4.20: Sun sensor data matches for rotation of GRBAAlpha.

We tried to find out how good the correlation is between our model and sensor measurements. Figure 4.21 shows correlations for all 5 sun sensors. Blue marks can be ignored, they correspond to a situation where the Sun is outside of the field of view of the sensor. Changes in measured values correspond only to albedo from the Earth, which is not simulated in our model. Therefore, these points are excluded from the simulation. We pay attention only to yellow points. As we can see, our rotation model predicts that the (X-) sensor is never illuminated. We also have some signal from (Z-) sensor, but less than the model predicts. There are some points where we predict signal (yellow points near the bottom), but it isn't measured in reality. This gives another reason, why model needs to be improved. In case of an ideal correlation, axes would have the same scales and all points would be on the diagonal.



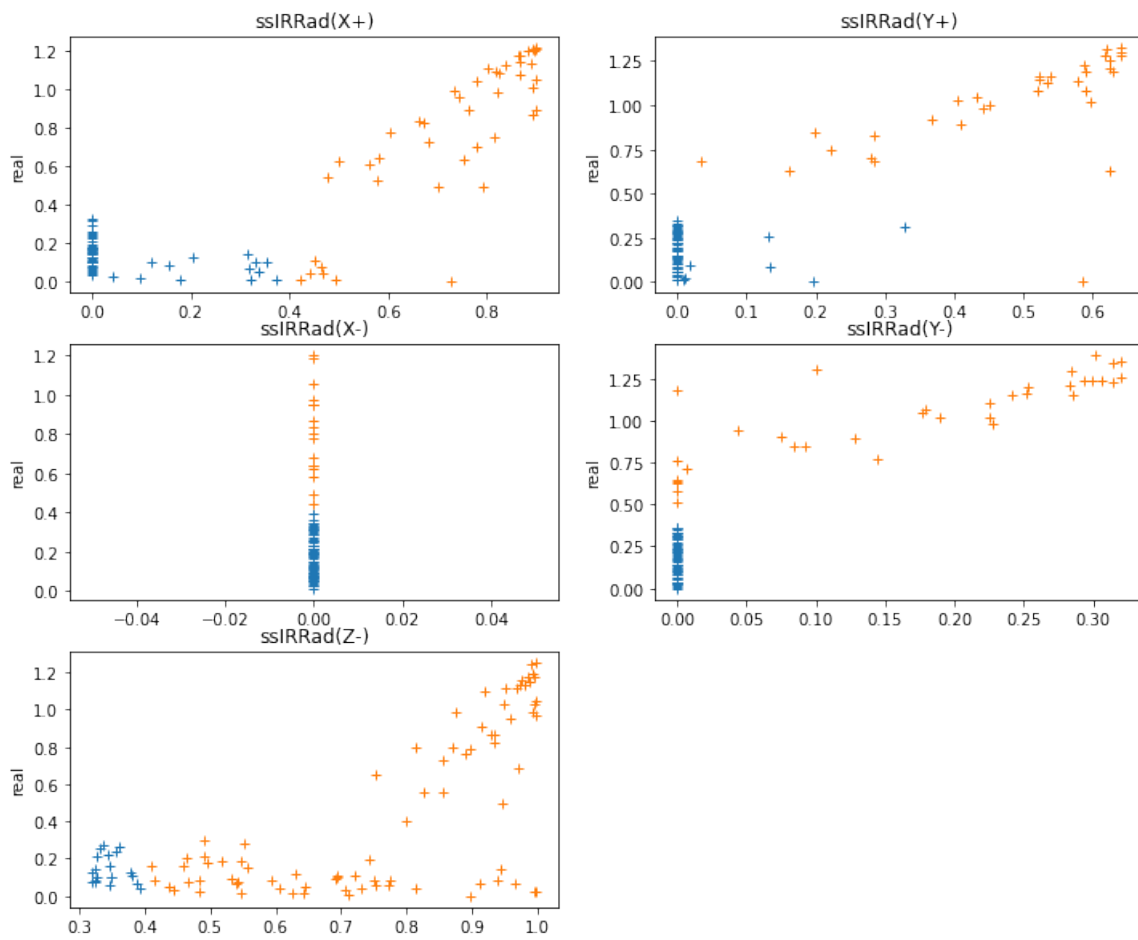


Figure 4.21: Model predictions and sensor measurements correlations.

We were not able to obtain much useful information about parameters of sun sensors from its manufacturer. We do not have calibration data nor a rough estimation of the field of view (where the signal drops for example by half or a quarter). We only know that data from sun sensors may be delayed by a few seconds by signal processing unit, but it doesn't matter for sun sensors as such. It can affect their alignment with magnetometer. For the purpose of the GRBAAlpha mission, where no active attitude orientation control system (AOCS) was integrated, the calibration of the satellite as a whole has not been done. Therefore, we created our own model, Figure 4.22, whose shape is to resemble real curves from sun sensors. Its parameters are the viewing angle on the X-axis and the sensitivity on the Y-axis, with a maximum of 30 000, which we determined from the approximate range of data shown in Figure 4.17. Parameters of the function, defined by formula 4.6, are in further studies adjusted to improve the model match. Then we simulated different roll angles for 5 sun sensors, for one rotation around a fixed magnetic axis. The output is Figure 4.23.

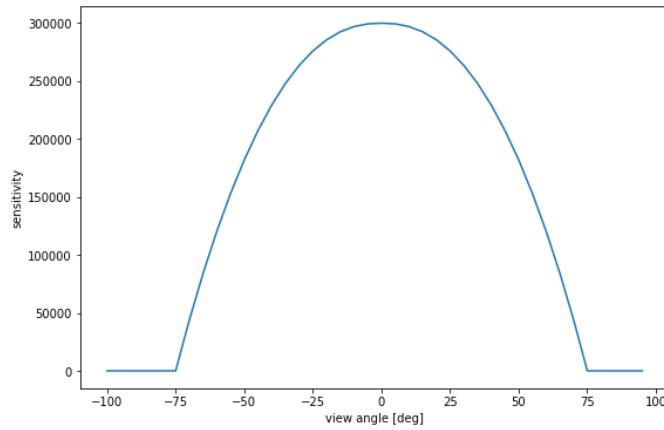


Figure 4.22: Model of sun sensor sensitivity function on view angle.

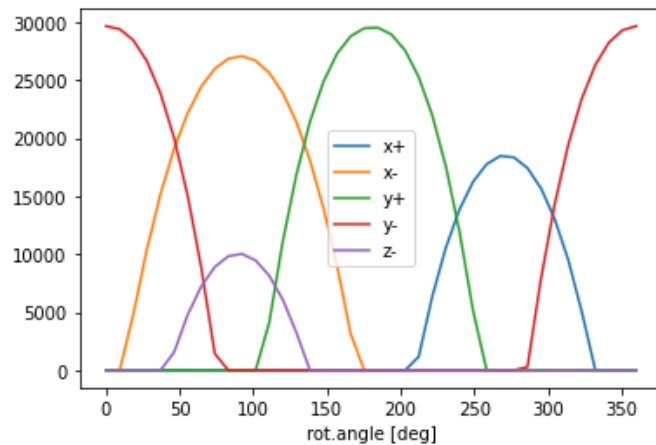


Figure 4.23: Simulation of one rotation along magnetic axis.

Model in Figure 4.22 is only two-dimensional. In reality, sun sensor may never be

pointing directly to the center of the Sun (as our model assumes at view angle of 0 degrees). Motion of the satellite may rotate the sensor closer to the Sun, but even when it reaches its maximal nominal value (for a specific position), it can still not be pointing directly at the Sun.

## 4.5 Upgraded model

Since our first model has not been really successful, we created a second one. We have now improved it by the view angle and by fitting two more parameters. Magnetic field is measured inside of GRBAAlpha body. We calculated a transformation matrix that converts magnetic field vector to the axis [0,0,1]. The magnetic axis is fixed, we rotated the satellite around it to find the best match with the sun sensor measurements. In the new model, the direction given by the magnetometer can slightly differ from ideal orientation – related to possible misalignment during sensor installation. We have defined two angles describing the inclination from the basic axis.

The Figure 4.24 shows effect of this inclination on one of the component of rotation matrix (calculated for every time from magnetometer direction and vector [0,0,1] in body frame): the matrix of original model is drawn in yellow, the new one in blue. The shift of "z-axis" vector here is less than 1 degree.

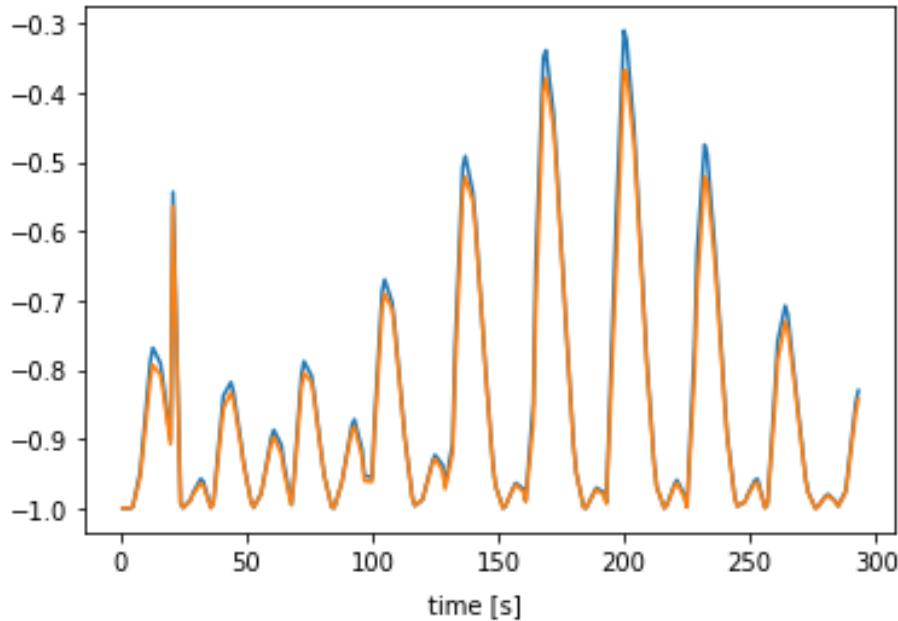


Figure 4.24: Effect of inclination on one of the component of rotation matrix.

Basic rotation function is given by equation (4.4):

$$\phi = 360^\circ \left( \frac{t}{T} + t^2 a \right) + \phi_0, \quad (4.4)$$

where  $\phi$  is basic rotation,  $t$  is time,  $T$  is period,  $a$  is an acceleration factor and  $\phi_0$  is phase. The modified rotation was calculated by equation (4.5):

$$\phi_m = \phi_r + \phi_s \sin(\phi_r - \phi_{dif}), \quad (4.5)$$

where  $\phi_m$  is modified rotation,  $\phi_r$  is small angle,  $\phi_s$  is an amplitude and  $\phi_{dif}$  is the difference between the beginning of the phase for normal shift and for sine function. The view angle function of sun sensor is modelled as follows:

$$V = A \left( 1 - \left( \frac{\alpha}{\beta} \right)^{exp} \right), \quad (4.6)$$

where  $V$  is a sensor signal at distance  $\alpha$  from normal axis,  $A$  is an amplitude,  $\beta$  is a limit angle and  $exp$  is a real exponent.

We also tried to predict phase with some sinusoidal modulation, final parameters are shown in Figure 4.25.

Table 4.2: Parameters for the first fit.

$$\begin{aligned} T &= 34.61 \text{ s} \\ \phi_0 &= 288.03 \text{ deg} \\ \phi_s &= 15.66 \text{ deg} \\ \phi_{dif} &= 203.07 \text{ deg} \\ a &= 1.42\text{e-}06 \text{ /s}^2 \end{aligned}$$

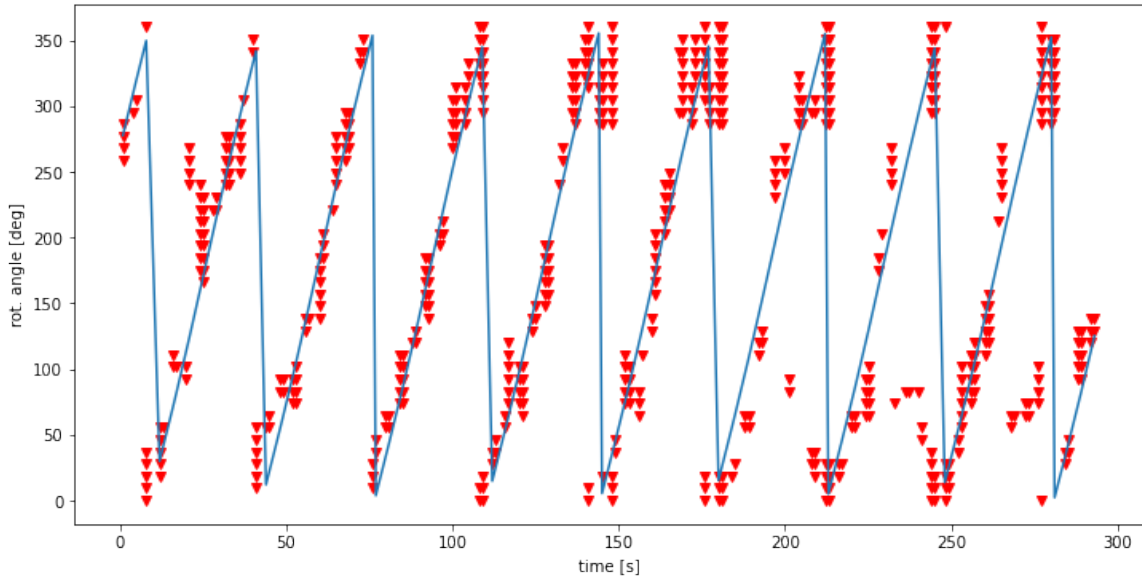


Figure 4.25: Development of rotation angle in time.

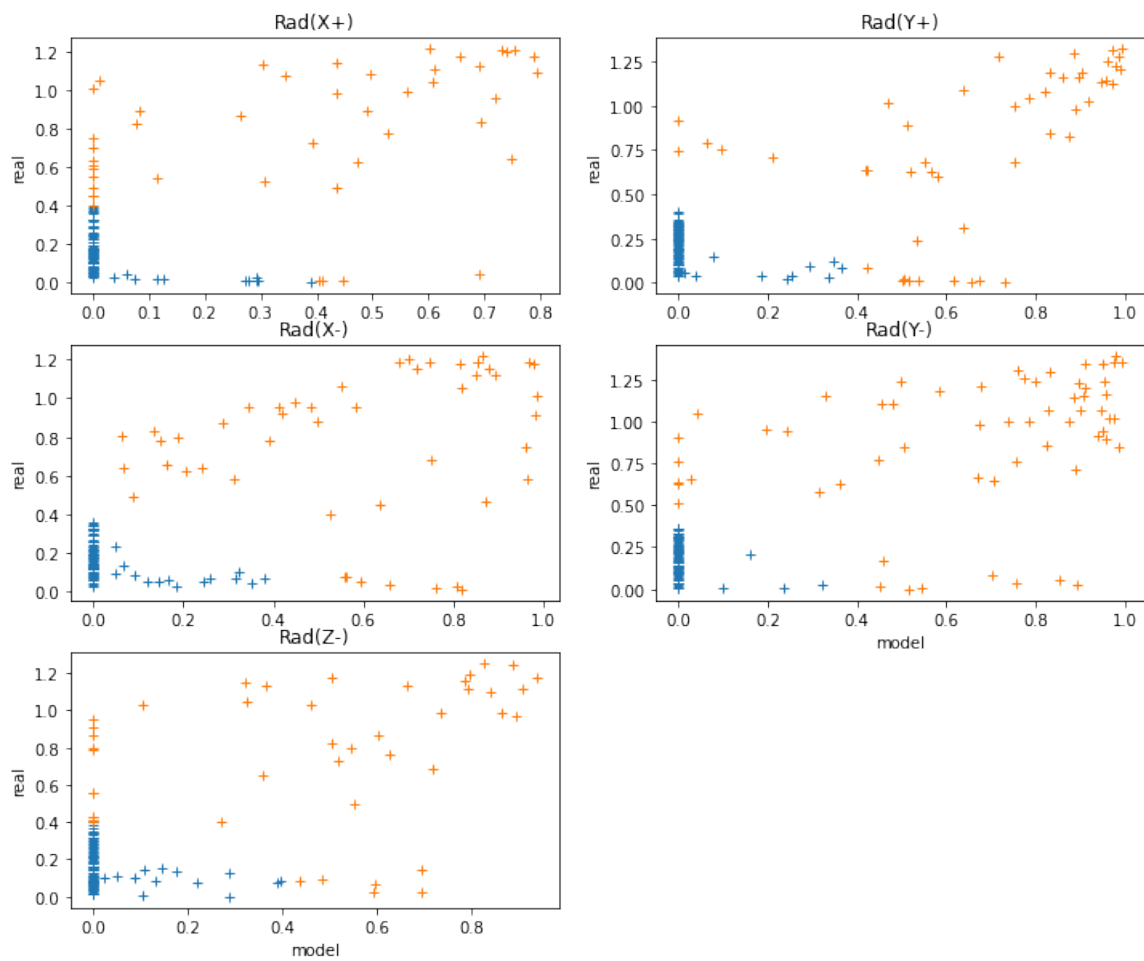


Figure 4.26: Second model predictions and sensor measurements correlations.

## 4.6 Third model

We have tried to apply the last model adjustment to a different merit function. During the measurements, different situations occurred for sun sensors. Sometimes we had a signal from one sensor at a given point in time, other times from two (rarely from three, or none at all). In our last model, we gave more weight to points (blue triangles), which represent the cases we have the signal from at least two sun sensors, both for points in the model and for measurements (Figure 4.27). All other triangles are red. Then we fitted the phase function 4.5 again. Our final view function is in Figure 4.28 and final correlation between sun sensors measurements and model is shown in Figure 4.29.

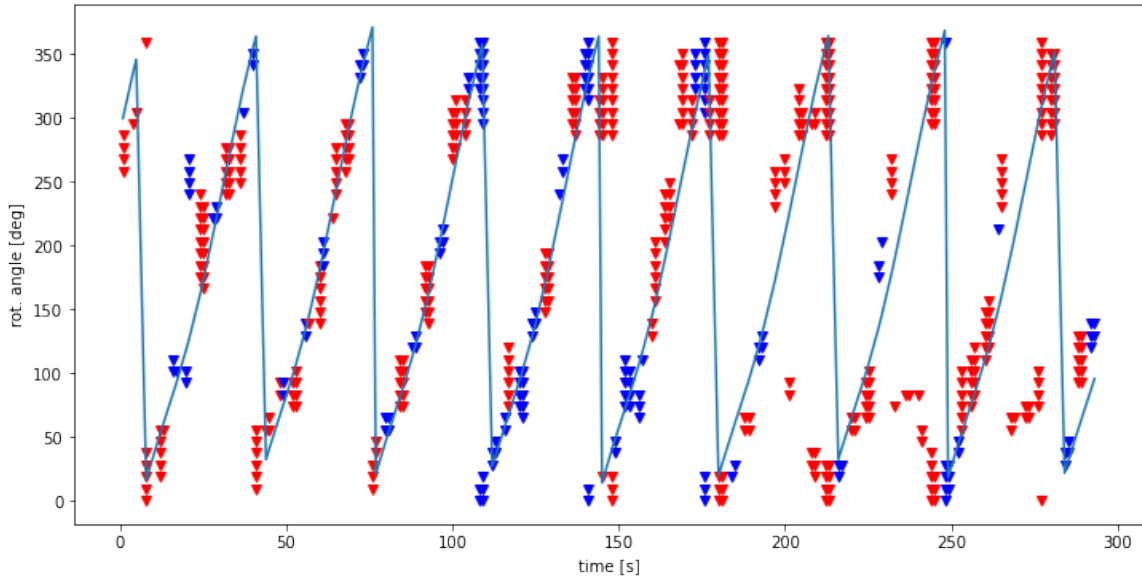


Figure 4.27: Development of rotation angle in time.

Table 4.3: Parameters for the best fit.

$T$	$=$	33.81	$\pm 0.03$ s
$\phi_0$	$=$	266.56	$\pm 0.76$ deg
$\phi_s$	$=$	8.39 deg	$\pm 0.18$ deg
$\phi_{dif}$	$=$	214.6	$\pm 3.5$ deg
$a$	$=$	$(-7.32 \pm 0.15) 10^{-7}$	$/s^2$
$\beta$	$=$	73.0	$\pm 0.5$ deg
$exp$	$=$	1.61	

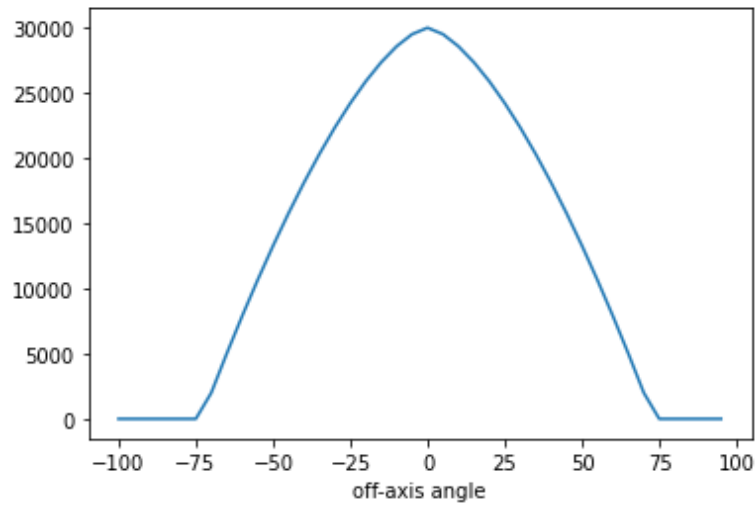


Figure 4.28: Final view function.

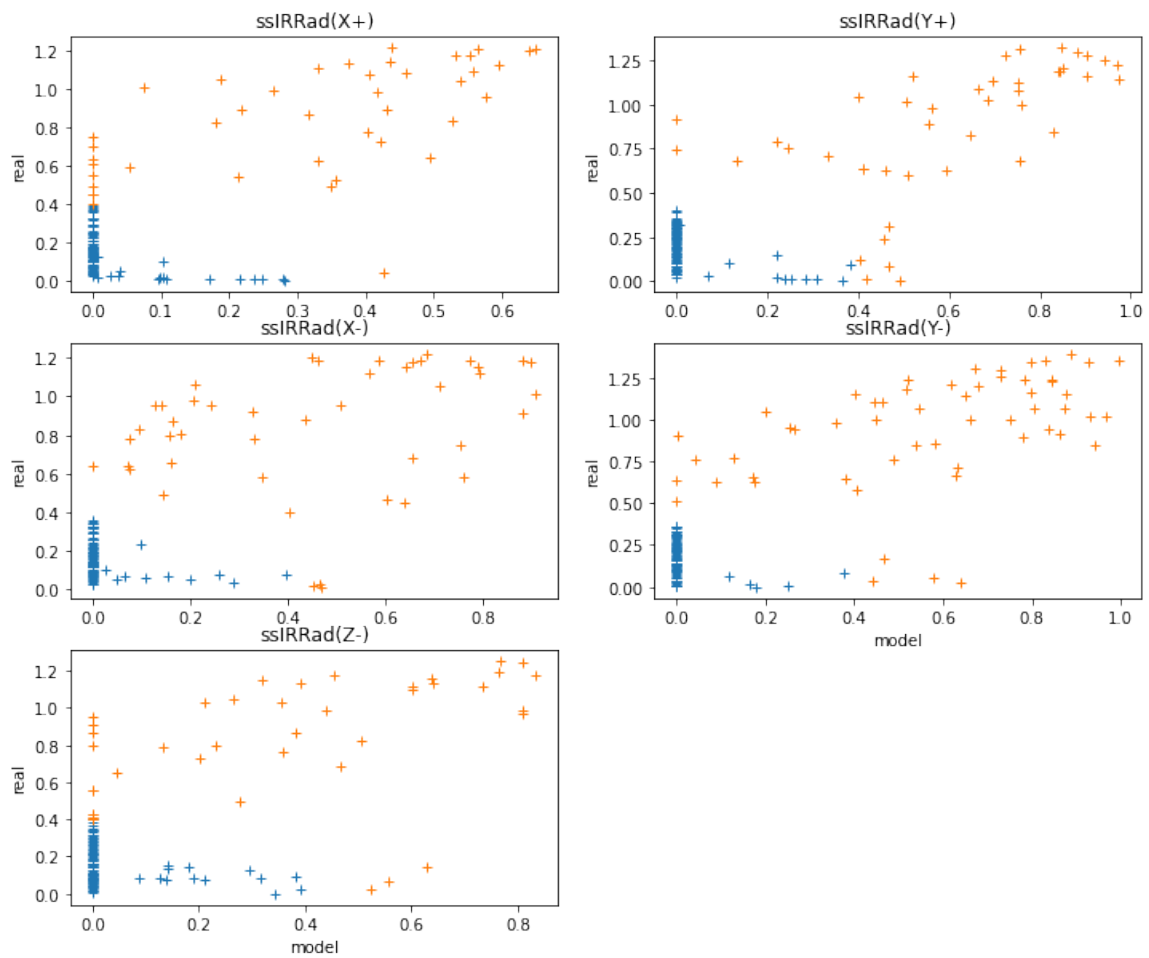


Figure 4.29: Final model predictions and sensor measurements correlations.

## 4.7 Computed attitude

When the Sun-direction model is complete, we have everything we need for the TRIAD method – two vectors in ECI, a magnetic vector directed in body frame, and the Sun-direction estimate given by the  $\phi_m$  function. From the two pairs of vectors, we calculate the rotation matrix, where the last column represents the coordinates of the vector Z. From its components  $x, y, z$  in the Cartesian coordinate system we can calculate its right ascension  $\alpha$  and declination  $\delta$  related by the equations bellow

$$\begin{aligned} x &= \cos \alpha \cos \delta, \\ y &= \sin \alpha \cos \delta, \\ z &= \sin \delta. \end{aligned} \tag{4.7}$$

Subsequently, we can plot the movement of the (Z+) axis component – Figure 4.30. We converted the directions to the individual axes in astropy from ECI to AltAz (NED). After this calculation we got Figure 4.32. The speed at which the individual axes rotate is drawn in Figure 4.33. Finally, we related the satellite orientation to its movement: the relative angle between the direction of motion of the satellite and the (Z+) axis is shown in Figure 4.34. It looks like the satellite is flying backwards. In fact, this corresponds to magnetometer measurements (Figure 4.5), where values for the Z axis are also negative.

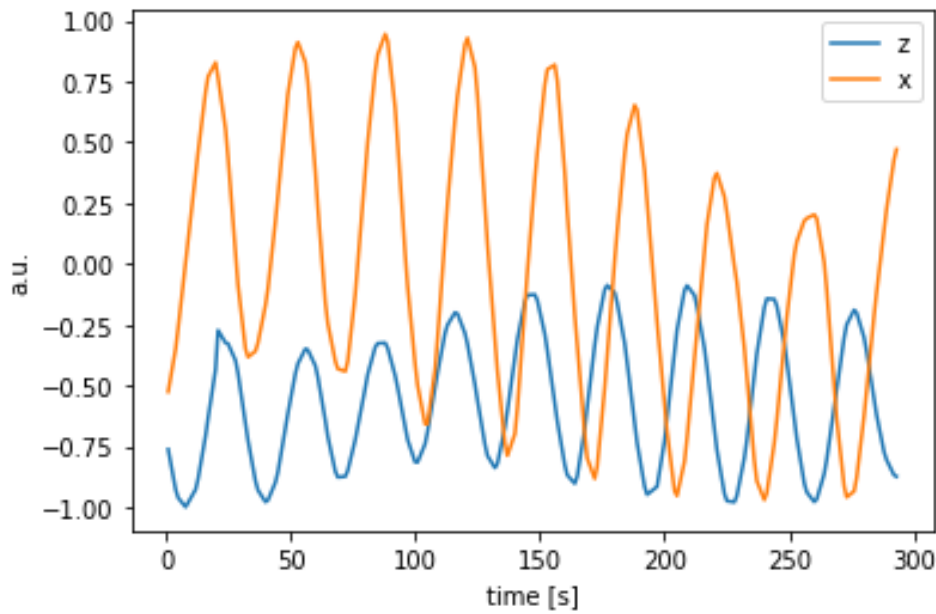


Figure 4.30: Movement of two (Z+) axis component.



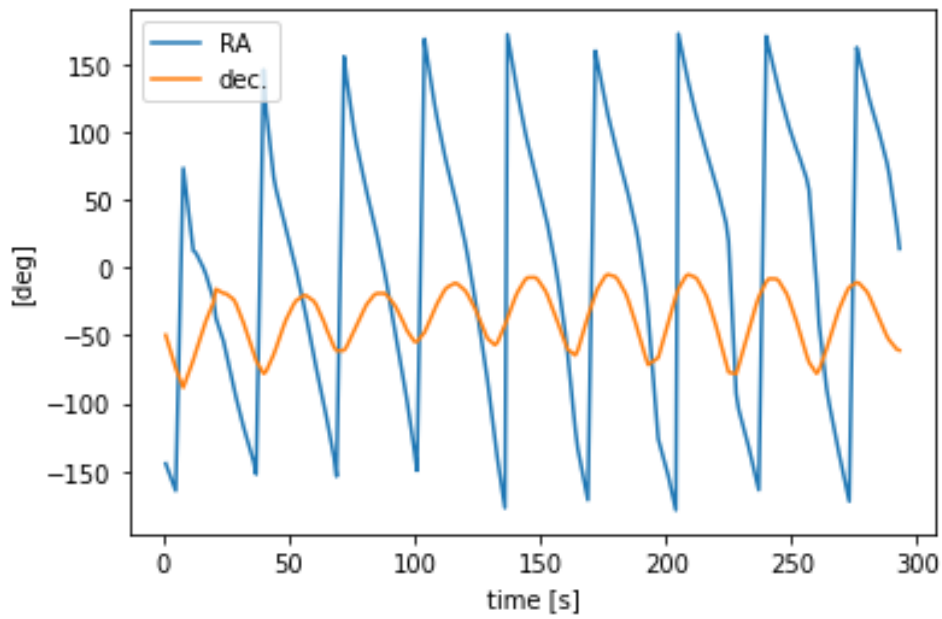


Figure 4.31: (Z+) axis, RA/DEC.

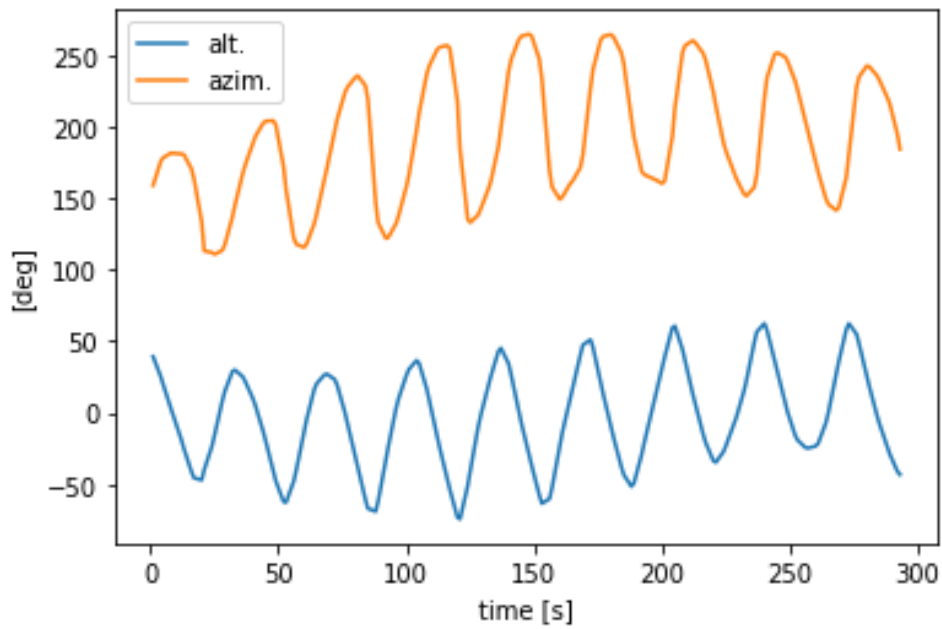


Figure 4.32: (Z+) axis in AltAz.

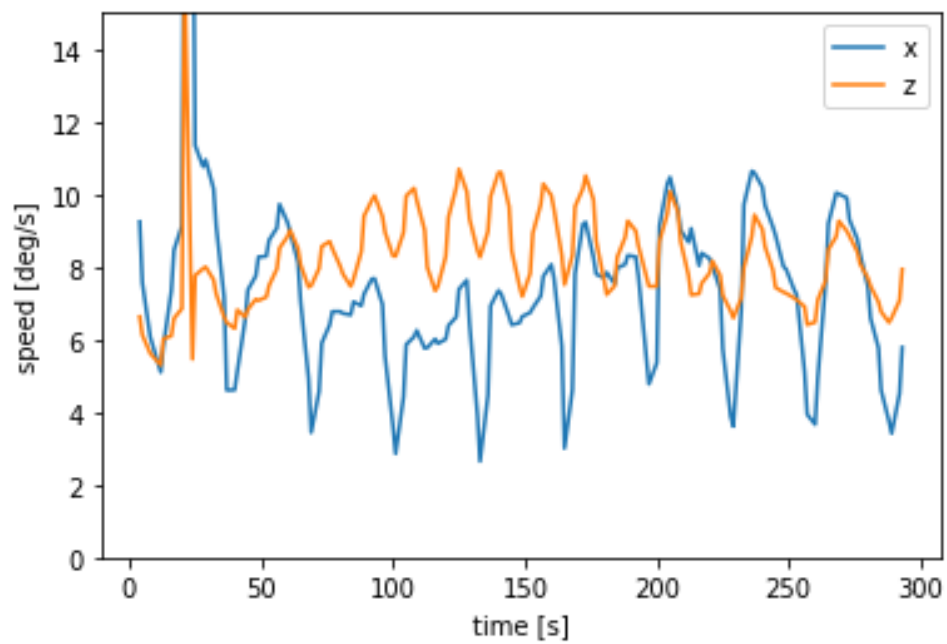


Figure 4.33: Speed of (X+) and (Z+) axis movement.

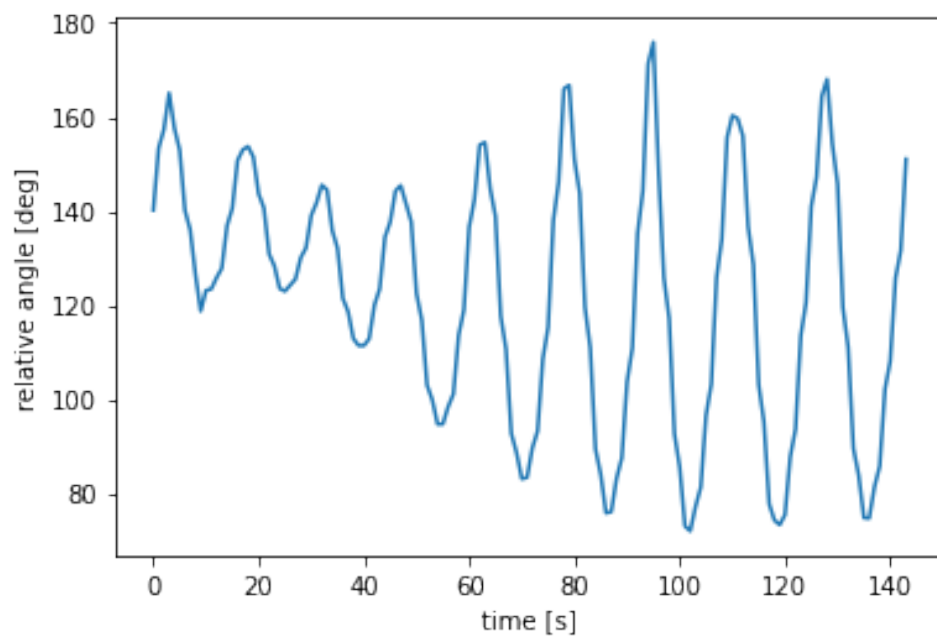


Figure 4.34: Relative angle between direction of movement and (Z+) axis.

# Conclusion

Our goal was to develop a method for determining nanosatellite (GRBAlpha) orientation using data from on board sensors and knowledge of satellite position from CelesTrak. Combining magnetometers and sun sensor data we could employ a TRIAD method.

We had an access to good data from magnetometers. However, sun sensors needed to be calibrated. Since we did not have enough information about them, we needed to develop our own calibration method. We corrected sensitivity of sun sensors, so that it was same in all directions (see Figures 4.15, 4.16, 4.18). Then we compared our model with real measurements using correlation (see Figure 4.21). We subsequently improved our first attempt of model by modifying a model view function (see Figure 4.22). Another (not very large) improvement was made by shifting the alignment of the measured magnetic vector with respect to the magnetic north of the Earth. We then defined the basic rotation function as equations (4.4) and the modified rotation function as equation (4.5), which we used to modify the satellite rotation model. Used parameters are in Table 4.2, the model of rotation of GRBAlpha in Figure 4.25 and the correlation of the new model with data measured by sun sensors is in Figure 4.26. In our final model, we optimized the parameters for equations (4.4, 4.5) and also optimized the view angle for equation (4.6) (see Table 4.3). The final view function is shown in Figure 4.28. We also gave more weight to points which presented a signal for at least two sun sensors (for both measured and model points).

After we computed all needed vectors, we performed the TRIAD transform and obtained a rotation matrix. The last column of this matrix represents coordinates of (Z) vector. We have shown the movements of this axis using its components in Figure 4.31. The orbit of the satellite is already shown in the figure 4.12. In Figure 4.34 there is drawn a relative angle between the direction of motion of the satellite and the (Z+) axis.

We were originally supposed to compare the data from GRBAlpha with the data from VZLUsat-2. This satellite, which was successfully launched in January 2022, is already equipped with set of reaction wheels to control its attitude. However, until now (after successful commissioning of the instruments aboard) VZLUsat-2 is not stabilized and it may take half a year for its operator team to learn to employ correctly its reaction wheels to reach complete stability. Its movement (as 3U CubeSat) is also fairly more complex than that of a 1U satellite like GRBAlpha.

The data used in this thesis do not contain data from the gamma-ray detector. Such measurements do exist, but not for the time when our data was measured. Signal modulation occurs only at specific times (when cosmic radiation shows strong anisotropy) and we do not have attitude data dense and accurate enough for any such period.

Development of our model would certainly benefit from a longer measurement, but after losing the VHF transmitter (one of 2 radios on board), scheduling such a measurement

is difficult (problem with command recording). Another problem is passive stabilization of the satellite, which was not successful enough. Even after a year on orbit, the satellite still performs rather violent movements.

Method described in our work could be refined e.g. by employing a sixth sun sensor, removing moments when no sensor sees Sun directly. In case of future CubeSats, the results of attitude determination would be definitely improved by a new generation of sun sensors that provide two-dimensional information about the Sun's position. In the future, it would also be interesting to find out what happens to the satellite as it passes near the magnetic poles. However, the description of its flipping would require a more complicated model.

# Bibliography

- [Bate et al. 1971] BATE, Roger R., Donald D. MUELLER and Jerry E. WHITE. 1971. *Fundamentals of Astrodynamics*. New York: Dover Publications, Inc.
- [Finance et al. 2021] FINANCE, Adrien, Christophe DUFOUR, Thomas BOUTÉRAON, Alain SARKISSIAN, Antoine MANGIN, Philippe KECKHUT and Mustapha MEFTAH. 2021. "In-Orbit Attitude Determination of the UVSQ-SAT CubeSat Using TRIAD and MEKF Methods." *Sensors* 21, no. 1: 7361. Accessible at: <https://doi.org/10.3390/s21217361>
- [Fortescue et al. 2003] FORTESCUE, Peter W. and Graham G. Swinerd. 2003. "Attitude Control." *In Spacecraft systems engineering*, edited by FORTESCUE, Peter W., John STARK and Graham G. SWINERD, 287-324. Hoboken: Wiley.
- [Frajt 2020] FRAJT, Marcel. 2020. "GRBAAlpha Attitude Coordination Document." *Spacemanic s.r.o.*, July 3, 2020.
- [Frajt 2021] FRAJT, Marcel. 2021. "GRBAAlpha Inertial properties analysis." *Spacemanic s.r.o.*, January 22, 2021.
- [Hall 2003] HALL, Christopher D. 2003. "Spacecraft Attitude Dynamics and Control." *Lecture Notes posted on Handouts page [online]* 12, no. 2003. Accessible at:
- [Hammen 2020] HAMMEN, David. 2020. "Reaction wheel and momentum wheel are near synonyms." *Stack Exchange*, May 12, 2020. Accessible at: <https://space.stackexchange.com/questions/25658/reaction-wheels-vs-momentum-wheels>
- [Hywel 2019] HYWEL, Curtis. 2019. "Satellite star trackers – the cutting edge celestial navigation products available on the global space marketplace." *Satsearch*. Last modified March 24, 2022. Accessible at: <https://blog.satsearch.co/2019-11-26-satellite-star-trackers-the-cutting-edge-celestial-navigation-products-available-on-the-global-space-marketplace>
- [Hywel 2020] HYWEL, Curtis. 2020. "Sun sensors on the global marketplace for space." *Satsearch*. Last modified March 24, 2022. Accessible at: <https://blog.satsearch.co/2020-02-12-sun-sensors-an-overview-of-systems-available-on-the-global-marketplace-for-space>

- [Kelecy et al. 2007] KELECY, Tom, Doyle HALL, Kris HAMADA and Maj. Dennis STOCKER. 2007. "Satellite Maneuver Detection Using Two-line Element ( TLE ) Data." In *Advanced Maui Optical and Space Surveillance Technologies Conference*, September 12-15, 2007, edited by S. Ryan, The Maui Economic Development Board. Accessible at: [https://www.researchgate.net/publication/242742404\\_Satellite\\_Maneuver\\_Detection\\_Using\\_Two-line\\_Elements\\_Data](https://www.researchgate.net/publication/242742404_Satellite_Maneuver_Detection_Using_Two-line_Elements_Data)
- [Makovec 2001] MAKOVEC, Kristin L. 2001. "A Nonlinear Magnetic Controller for Three-Axis Stability of Nanosatellites." Master's thesis, Faculty of the Virginia Polytechnic Institute and State University. Accessible at: <https://vtechworks.lib.vt.edu/handle/10919/34131>
- [Řípa et al. 2021] ŘÍPA, Jakub, Masanori OHNO, Hiromitsu TAKAHASHI, András PAL, L. MESZAROS, Norbert WERNER, Martin TOPINKA et al. 2021. "GRB 211018A: Detection by GRBAlpha." GRB Coordinates Network, Circular Service, No. 30945. Accessible at: <https://ui.adsabs.harvard.edu/abs/2021GCN.30945....1O/abstract>
- [Pál et al. 2020] PÁL, András, Masanori OHNO, László MÉSZÁROS, Norbert WERNER, Jakub ŘÍPA, Marcel FRAJT, Naoyoshi HIRADE et al. 2020. "GRBAlpha: A 1U CubeSat mission for validating timing-based gamma-ray burst localization.", *Proc. SPIE 11444, Space Telescopes and Instrumentation 2020*
- [Rawashed 2010] RAWASHED, Samir A. 2010. "PASSIVE ATTITUDE STABILIZATION FOR SMALL SATELLITES." Master's thesis, University of Kentucky. Accessible at: [https://uknowledge.uky.edu/gradschool\\_theses/624](https://uknowledge.uky.edu/gradschool_theses/624)
- [Riebeek 2009] RIEBEEK, Holli. 2009. "Catalog of Earth Satellite Orbits." *NASA Earth Observatory*, September 4, 2009. Accessible at: <https://earthobservatory.nasa.gov/features/OrbitsCatalog>
- [Řípa 2021] ŘÍPA, Jakub. 2021. GRB211018A. Digital eps diagram. Measured on 18<sup>th</sup> of October 2021, 22:25:52 UTC. GRBAplha, INTEGRAL-SPI-ASC.
- [Shuster et al. 2005] SHUSTER, Malcolm D. and Wayne F. DELLINGER. 2005. "Spacecraft Attitude Determination and Control." In *Fundamentals of Space Systems: second edition*, edited by PISACANE, Vincent L., 236-325. New York: Oxford University Press.
- [Sidi 1997] SIDI, Marcel J. 1997. *Spacecraft Dynamics and Control: A Practical Engineering Approach (Cambridge Aerospace Series)*. Cambridge: Cambridge University Press. Accessible at: <https://doi.org/10.1017/CBO9780511815652>
- [Snay et al. 1999] SNAY, Richard A. and Thomas SOLER. 1999. "Modern Terrestrial Reference Systems (Part 1)." *Professional Surveyor* 19, no. 10: 32-33. Accessible at: <https://www.ngs.noaa.gov/CORS/Articles/>
- [Sumathi et al. 2013] SUMATHI, Manickam, Ravi RANJAN, Ramesh Kumar SINGH and Prashant KUMAR. 2013. "Performance analysis of sun sensors for satellite systems."

*International Conference on Advanced Electronic Systems (ICAES)*, 2013: 10-14.  
Accessible at: 10.1109/ICAES.2013.6659351

[Werner et al. 2018] WERNER, Norbert, Jakub ŘÍPA, András PAL, Masanori OHNO, Norbert TARCAI, Kento TORIGOE, Koji TANAKA et al. 2018. "CAMELOT: Cubesats Applied for MEasuring and LOcalising Transients - Mission Overview." In DenHerder, JWA; Nikzad, S. Nakazawa, K. SPACE TELESCOPES AND INSTRUMENTATION 2018: ULTRAVIOLET TO GAMMA RAY. BELLINGHAM: SPIE-INT SOC OPTICAL ENGINEERING, 2018: 1-15. Accessible at: doi:10.1117/12.2313764

[Zafar et al. 2019] ZAFAR, Saniya, Haroon IBRAHIM and Khurram KHURSHID. 2019. "Earth horizon sensor for attitude determination of LEO satellites." *Second International Conference on Latest trends in Electrical Engineering and Computing Technologies (INTELLECT)*, 2019: 1-6. Accessible at: 10.1109/INTELLECT47034.2019.8955456

[Zheng 2017] ZHENG, You. 2017. *Space Microsystems and Micro/Nano Satellites*. Oxford: Butterworth-Heinemann.

# Appendix A

## GRB Alpha

On 22<sup>nd</sup> of March 2021, the Czech-Slovak-Japanese-Hungarian GRBAlpha satellite was launched from Baikonur in Kazakhstan on the Soyuz-2 launch vehicle. It is a 1U CubeSat nanosatellite with a weight of 1195 g and size of 100x100x113.5 mm. The name GRB is based on Gamma Ray Burst, and Alpha means that this is the first mission of a gamma-ray bursts detector. Gamma-ray detector is made of caesium iodide crystal with dimensions of 75x75x0.5 mm, the scintillation photons are recorded by Multi-pixel Photon Counter (MPPC or SiPM) sensors in 2 separate channels. This detector was developed in a frame of a future CubeSat constellation called CAMELOT (Werner et al. 2018), while other nanosatellite components were integrated by Spacemanic company ([spacemanic.com](https://www.spacemanic.com)<sup>5</sup>).

The satellite was built by a collaboration led by Konkoly Observatory of the Eötvös Loránd Research Network along with Hiroshima University, Spacemanic s.r.o., Needronix s.r.o., Eötvös University, Nagoya University, Masaryk University and Brno University of Technology while the launch contract and radio license is provided by Technical University of Košice ([online](https://grbalpha.konkoly.hu/)<sup>6</sup>).

## Coordinate system of satellite

Coordinate system of the satellite is essential for development of the attitude determination and control system (ADCS) algorithms. The origin of the coordinate system is shown in Figure A.1. It is a right-hand coordinate system located in the corner of the satellite. The X-axis is shown in red, the y-axis in green, and the z-axis in blue (Frajt 2020, p. 5).

---

<sup>5</sup>Online: <https://www.spacemanic.com/missions/grbalpha/>

<sup>6</sup>Online: <https://grbalpha.konkoly.hu/>



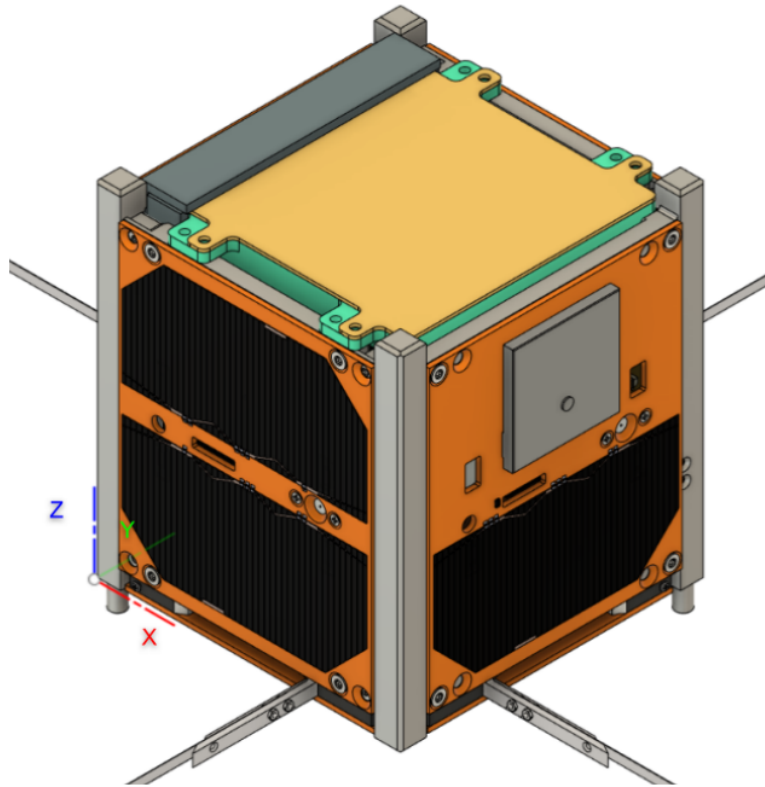


Figure A.1: Coordinate system of GRBAAlpha ([Frajt 2020](#)).

## Sun sensor coordination

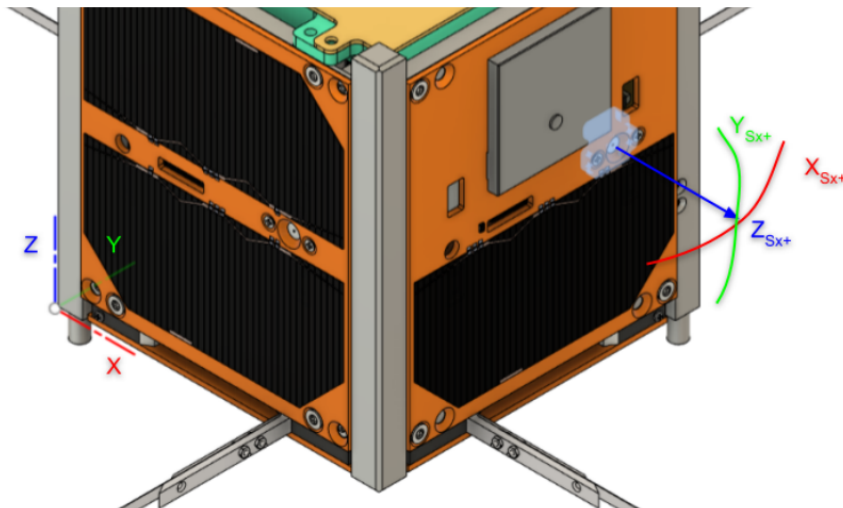


Figure A.2: The XY plane of Sun sensor  $X_+$  is parallel to the YZ satellite plane. Sun sensor Z axis united with satellite  $X_+$  axis ([Frajt 2020](#)).

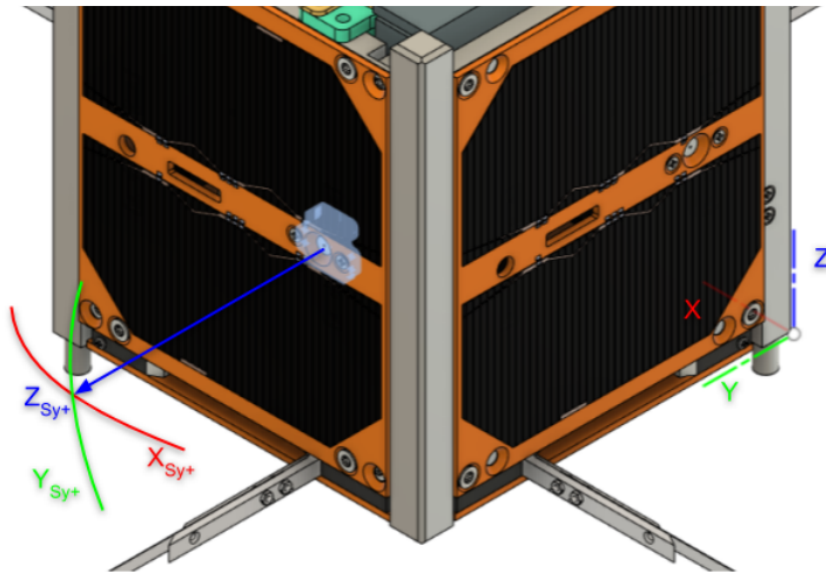


Figure A.3: The XY plane of Sun sensor Y+ is parallel to the XZ satellite plane. Sun sensor Z axis united with satellite Y+ axis (Frajt 2020).

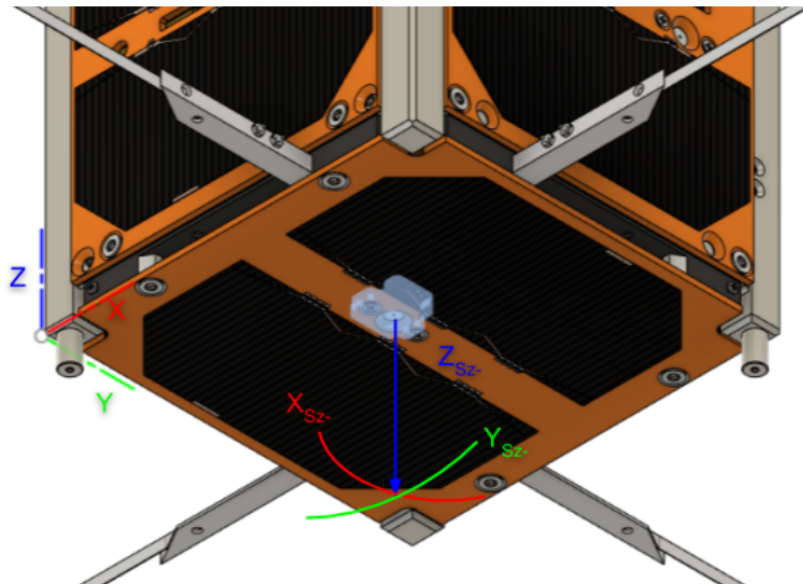


Figure A.4: The XY plane of Sun sensor Z- is parallel to the XY satellite plane. Sun sensor Z axis united with satellite Z- axis (Frajt 2020).

## Satellite design

Components of the satellite are the power supply unit (from [GOMspace<sup>7</sup>](https://gomspace.com/home.aspx)), the on-board computer, very high frequency (VHF) and ultra high frequency (UHF) transceivers (from [Needronix<sup>8</sup>](https://needronix.eu/)) and the GPS receiver (from [Spacemanic<sup>9</sup>](https://www.spacemanic.com/)). There is also a sensor board with sun-sensors (from [Needronix](https://needronix.eu/)), magnetometers, thermometers, gyroscopes and a space X-ray dosimeter (Space X-ray Detector (SXD) from [VZLÚ<sup>10</sup>](https://www.vzlu.cz/?lang=en)). The satellite uses the CubeSat protocol to perform internal communication. It is the communication between various components of the payload and the platform. These components are shown in Figure A.5 and Figure A.6.

Permanent magnets are used to passively detumble the satellite. However, orientation data are needed to interpret the scintillator data correctly. These are provided by small sun sensors on five sides of the satellite (X+, Y+, X-, Y- and Z-) and an inertial measurement unit (IMU) employing gyroscopes and accelerometers ([Pál et al. 2020](#)).

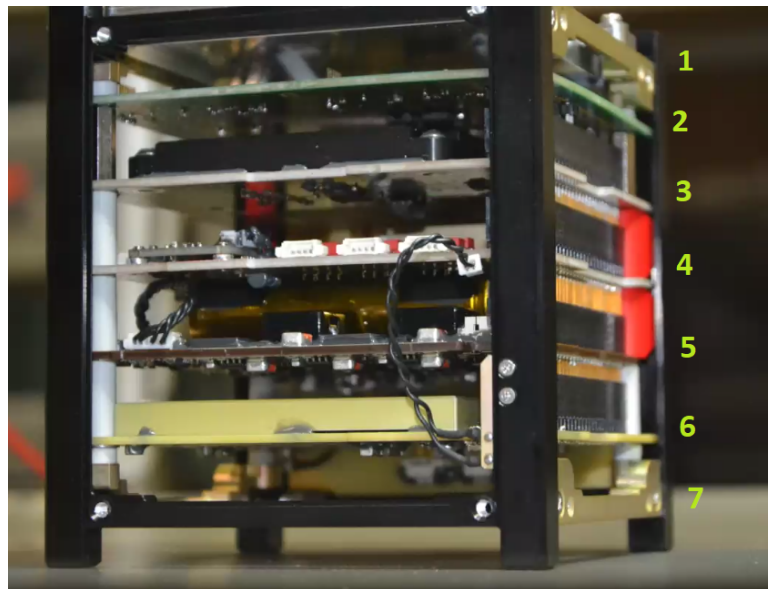


Figure A.5: Internal components of the GRBAlpha satellite. From Z + to Z in this image: 1. scintillator housing; 2. dual channel payload board; 3. board supporting onboard computer and GPS receiver; 4. sensor board; 5. power supply; 6. dual UHF, VHF transceiver module; 7. deployable antennas. Credits: Spacemanic

<sup>7</sup>Online: <https://gomspace.com/home.aspx>

<sup>8</sup>Online: <https://needronix.eu/>

<sup>9</sup>Online: <https://www.spacemanic.com/>

<sup>10</sup>Online: <https://www.vzlu.cz/?lang=en>



Figure A.6: Internal components of the GRBAAlpha satellite. 1. Scintillator; 2. electronics; 3. onboard computer + GPS; 4. Lodestone and X-ray detector (X-ray dosimeter from VZLÚ); 5. power supply module with batteries; 6. UHF and VHF transceiver; 7. antenna mount; 8., 9. solar panels; 10. frames (Pál et al. 2020).

## Scintillator

The scintillator is an essential part of the gamma-ray detector, which is able to detect sources in the range of 30-900 keV. It produces scintillation photons that are registered with multi-pixel silicon photomultipliers (MPPC S13360-3050CS as for Multi-Pixel Photon Counter from Hamamatsu<sup>11</sup>). Eight of these MPCCs are glued to the scintillation crystal.

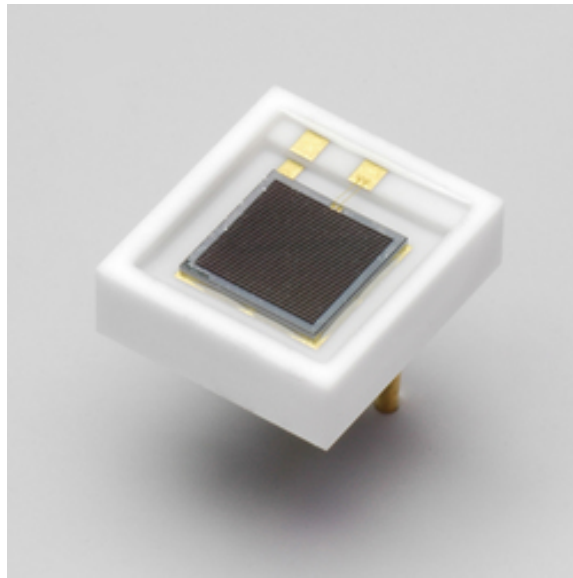


Figure A.7: MPPC S13360-3050CS from Hamamatsu.

<sup>11</sup>Online: [https://www.hamamatsu.com/us/en/product/optical-sensors/mppc/mppc\\_mppc\\_array/S13360-3050CS.html](https://www.hamamatsu.com/us/en/product/optical-sensors/mppc/mppc_mppc_array/S13360-3050CS.html)

## Lodestone

Operating temperature:  $-40\text{ }^{\circ}\text{C}$  to  $+85\text{ }^{\circ}\text{C}$ .

Power Supply: 3.3 V.

Size: 22x20x5 mm.

3-axis gyroscope and 3-axis magnetometer in one module

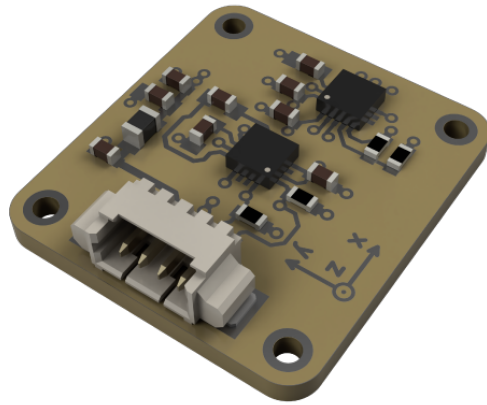


Figure A.8: Lodestone from Spacemanic ([spacemanic.com](http://spacemanic.com)).

## Solar panels

Operating temperature:  $-40\text{ }^{\circ}\text{C}$  to  $+125\text{ }^{\circ}\text{C}$ .

Mass: 50 g (1U).

Thickness: 1.6 mm  $\pm$  10 % .

Photodiode: 5° heading accuracy.

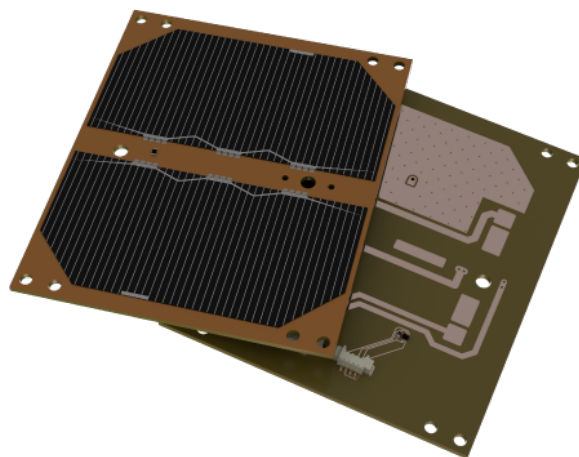


Figure A.9: Solar panels from Spacemanic ([spacemanic.com](http://spacemanic.com)).

## UHF, VHF transceivers

Frequency range: 145-440 MHz.

Analog input (max): 2.5 V.

Sensitivity:  $< -100$  dB.

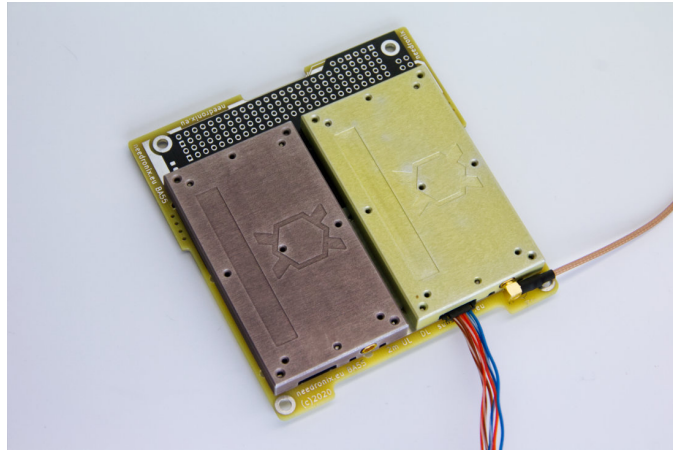


Figure A.10: UHF and VHF transceivers from Needronix ([needronix.eu](http://needronix.eu)).

## Power supply unit

Size: 40x70x6.5 mm

Battery voltage 8 V.

Onboard battery: 20 Wh.

Photovoltaic power conversion up to 30 W.



Figure A.11: Power supply unit from GOMspace ([gomspace.com](http://gomspace.com)).

## Onboard computer

On-board gyro/mag/acc sensors.

Operating temperature:  $-40\text{ }^{\circ}\text{C}$  to  $+85\text{ }^{\circ}\text{C}$ .

Power Supply: 3.3 V, 5 V, 3.3 V isolated.

Mass: 25 g.

Power consumption: 100 mW average .

## Sun sensors

Type: NXSS3v00.

Size: 15,5x15x4,7 mm.

Weight: 3 g.

Operating temperature:  $-40\text{ }^{\circ}\text{C}$  to  $86\text{ }^{\circ}\text{C}$ .

Field of view:  $> 100\text{ deg}$ .

Input voltage: 2–3,6 V.

Input current:

$< 2\text{ mA}$  (activemode),

$< 500\text{ }\mu\text{A}$  (sleepmode when exposed to the sun),

$< 20\text{ }\mu\text{A}$  (sleepmode in the dark).



Figure A.12: Onboard computer from Spacemanic ([spacemanic.com](http://spacemanic.com)).

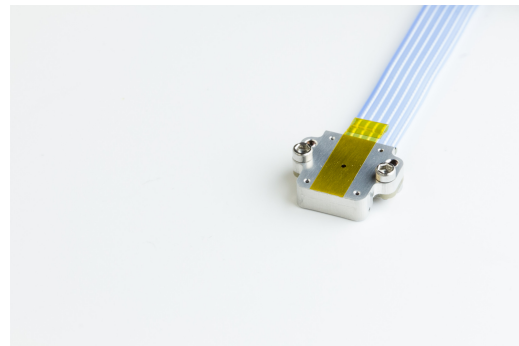


Figure A.13: Sun sensors from Nee-dronix ([sunsensors.eu](http://sunsensors.eu)).



## Permanent magnets

A set of permanent magnets is used for passive stabilization of GRBA $\alpha$ . The magnets are embedded in red plastic holders on the sides of the satellite, as shown in Figure A.14. The north of the magnet corresponds to the direction of the Z+ axis of the satellite coordinate system. Three orthogonal sheets (each of 0.134 cm<sup>3</sup>) of special high-hysteresis material (brand HyMu80<sup>12</sup>, previously used also on US KySat-1 nanosatellite) is used to slowly damp oscillations of the satellite. Total magnetic dipole of used magnets is 1.37 Am<sup>2</sup>.

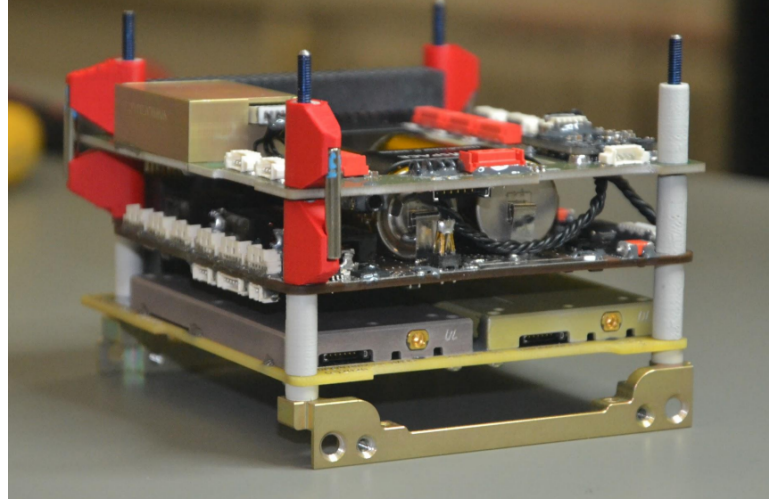


Figure A.14: Permanent magnets (Frajt 2020, p. 15).

## Center of mass

The position of the center of mass (the center of gravity) is in relation to geometrical center at X: -0.95mm, Y: -2.49mm and Z: 5.97mm. (Frajt 2021, p. 6). The mass moments of inertia are estimated at:

Table 1: The mass moments of inertia (Frajt 2021, p. 6).

Ixx:	0.002 kg m <sup>2</sup> $\pm$ 10%
Iyy:	0.002 kg m <sup>2</sup> $\pm$ 10%
Izz:	0.002 kg m <sup>2</sup> $\pm$ 10%
Ixy:	0.000 kg m <sup>2</sup> $\pm$ 10%
Ixz:	0.000 kg m <sup>2</sup> $\pm$ 10%
Iyz:	0.000 kg m <sup>2</sup> $\pm$ 10%

<sup>12</sup>Online: [https://www.nealloys.com/hymu\\_80.php](https://www.nealloys.com/hymu_80.php)



# Appendix B

GRBAAlpha is a Low Earth Orbit (LEO) satellite with a polar orbit. It orbits the Earth approximately every 90 minutes. During the flight over the ground stations, the devices have only a limited time to transmit the acquired data till it falls beyond horizon. Communication occurs as soon as it goes above the horizon. What does such a transmission look like? A nice example are the so-called Waterfalls. These are figures that show the signal strength depending on the radio frequency and time. The rough green part in the middle represents the time when the satellite was transmitting data. The following figure is an example of such a Waterfall. This is a transmission from GRBAAlpha with time frame from April 6<sup>th</sup> 2022 (09:00:22 to 09:12:35). The satellite was transmitting at a frequency of 437.025 MHz.

Doppler correction is also applied: relative speed of the satellite and the station is taken into account and the frequency on which the ground station transmits is adjusted. The faint green "S" in the background of the waterfall Figure B.1 is caused by the above-mentioned correction made by the transmitting ground station recorded by another not-so-distant station.

The dark bands in the green broadcast are unfavorably rotated antennas of GRBAAlpha. These cause gaps in the transmission. With a better study of the distances between the gaps, it is possible to find the period in them. Here we assume that the satellite initially spun and eventually stabilized using the passive method. The question is whether, in the case of a sufficiently dense measurement, we can reveal how the satellite tumbles. With this information, we can correct variation of sensitivity in the light curve of sources of gamma-ray burst. Stabilized satellites obviously measure gamma-ray lightcurves more reliably. An example is the detection of burst GRB211018A (Figure B.2) from the work of J. Řípa, who showed an overlay of the data measured by GRBAAlpha and INTEGRAL SPI anticoincidence system (ACS) (Řípa et al. 2021).

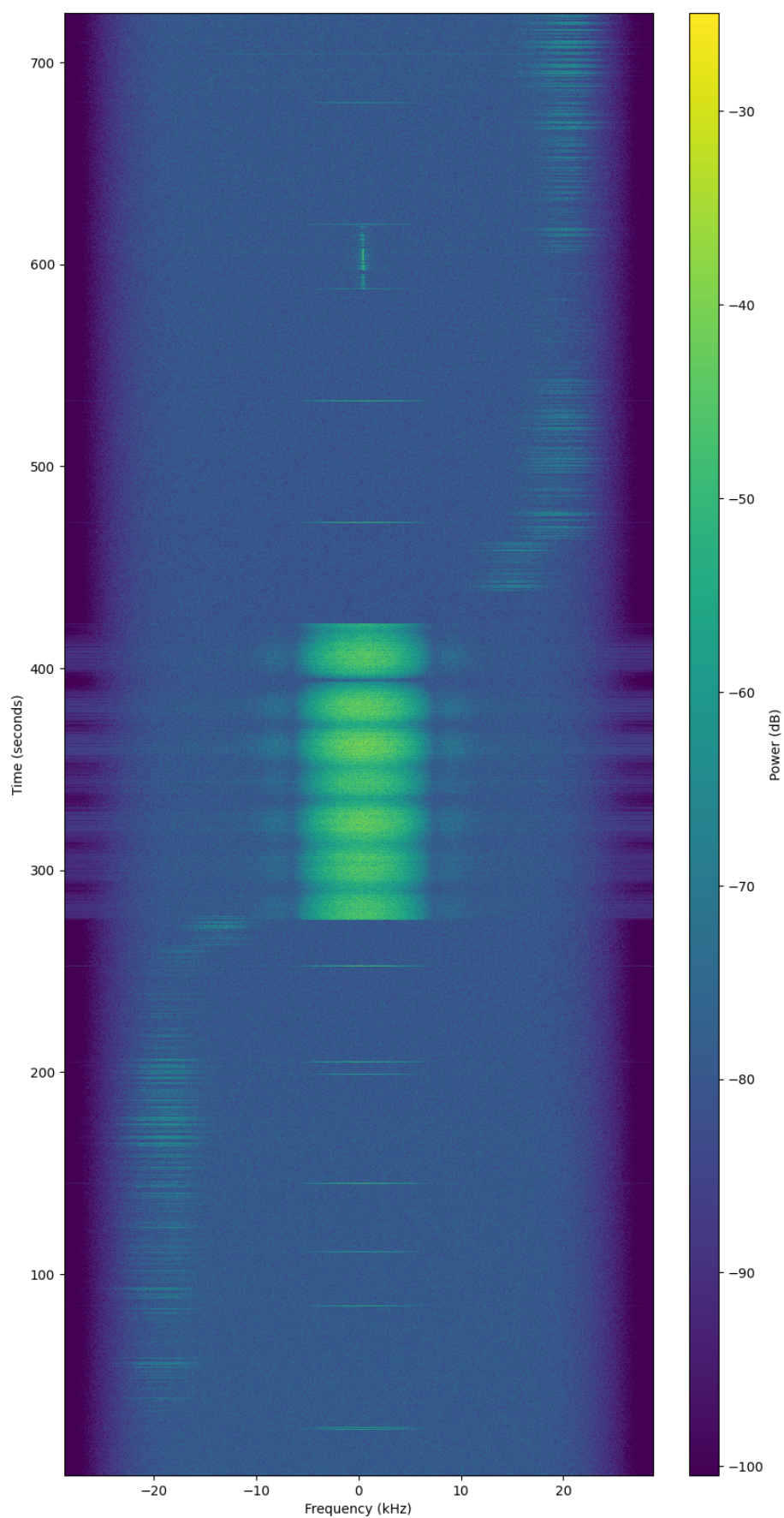


Figure B.1: Waterfall. Station Piszkesteto UHF, Hungary. April 6<sup>th</sup> 2022.

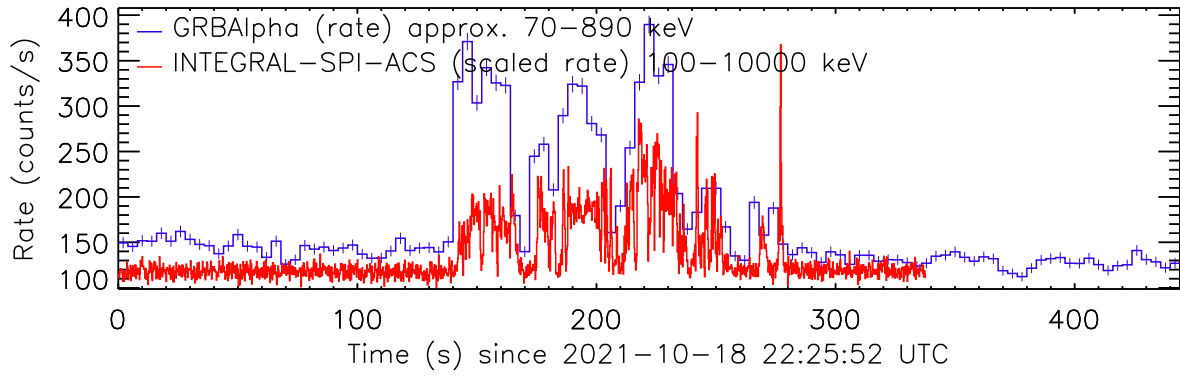


Figure B.2: GRB211018A. Comparison of measurements from GRBApha and INTEGRAL-SPI-ACS ([Řípa 2021](#)).

